Materials & Design 216 (2022) 110551

Contents lists available at ScienceDirect

Materials & Design

journal homepage: www.elsevier.com/locate/matdes

A universally dispersible graphene-based ink modifier facilitates 3D printing of multi-functional tissue-engineered scaffolds

Chengshen Hu [a,b,c], Zhigang Chen [a], Lan Tang [a,b], Juan Liu [a], Jirong Yang [a], Wing-Fu Lai [d,e], Tong Wu [a], Siyuan Liao [b], Xintao Zhang [f], Haobo Pan [a,b], Changshun Ruan [a,b,*]

[a] Research Center for Human Tissue and Organs Degeneration, Institute of Biomedicine and Biotechnology, Shenzhen Institute of Advanced Technology, Chinese Academy of Sciences, Shenzhen 518055, PR China
[b] University of Chinese Academy of Sciences, Beijing 100049, PR China
[c] Department of Chemistry in Tangtou Campus, Baoan Middle School (Group), Shenzhen 518101, PR China
[d] School of Life and Health Sciences, The Chinese University of Hong Kong (Shenzhen), Shenzhen 518172, PR China
[e] Department of Applied Biology and Chemical Technology, Hong Kong Polytechnic University, Hong Kong Special Administrative Region
[f] Department of Sports Medicine and Rehabilitation, Peking University Shenzhen Hospital, Shenzhen 518036, PR China

HIGHLIGHTS

- A universally dispersible graphene oxide-based polyurethane (GO-PU) is successfully prepared.
- This GO-PU can be used as an ink modifier to endow the arbitrary bioink matrixes with better mechanical properties and multifunction.
- In vitro and in vivo toxicity test showed that GO-PU has excellent biocompatibility.

GRAPHICAL ABSTRACT

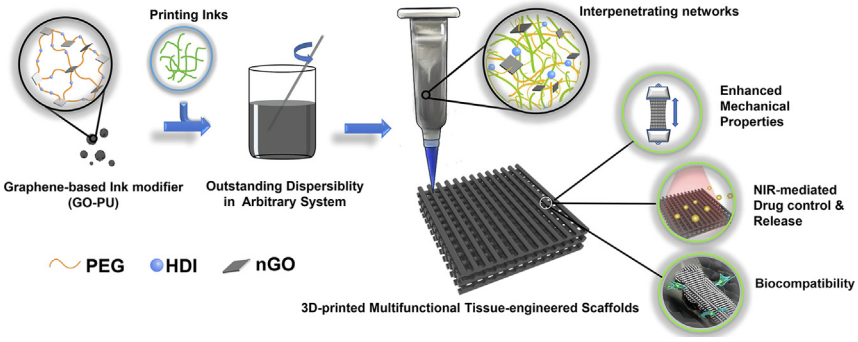

ARTICLE INFO

Article history:
Received 13 February 2021
Revised 21 February 2022
Accepted 13 March 2022
Available online 16 March 2022

Keywords:
3D-printing ink modifier
Polyurethane
Graphene oxide
Dispersity
Tissue-engineered scaffolds

ABSTRACT

3D-printed bioscaffolds for the realization of individualized tissue regeneration remains challenging due to the limitation in terms of current biomaterial inks. Exploring a universal ink modifier to enhance the properties of the arbitrary inks for 3D printing of multi-functional scaffolds is therefore an alternative. Herein, a universally dispersible graphene oxide-based polyurethane (GO-PU) ink modifier with network structure constituting amphiphilic polyethylene glycol (PEG) and nanoscale GO (nGO) is presented for the first time. GO-PU can be stably dispersed in various organic and aqueous solutions for 24 h without obvious aggregation, far superior to pure nGO. The excellent printability of GO-PU is demonstrated to fabricate pure GO-PU and GO-PU modified composite scaffolds in which GO-PU is used as ink modifiers. The addition of GO-PU with 5% (ww%/wt%) contents into PLGA or PEGDA can not only improve their mechanical properties without decrease printability, but also endow the additional performances with the resulting scaffolds from the incorporated functional nGO segments, like photo-triggered release ability. In addition, the results of *in vitro* and *in vivo* toxicity tests confirmed that GO-PU is biocompatible, indicating that this facile and universal approach for introducing graphene materials into 3D-printed scaffolds is with a great potential for tissue regeneration.

* Corresponding author at: Research Center for Human Tissue and Organs Degeneration, Institute of Biomedicine and Biotechnology, Shenzhen Institute of Advanced Technology, Chinese Academy of Sciences, Shenzhen 518055, PR China.
E-mail address: cs.ruan@siat.ac.cn (C. Ruan).

https://doi.org/10.1016/j.matdes.2022.110551
0264-1275/

1. Introduction

Biomaterial-based scaffolds with controllable structure, satisfactory mechanical properties, excellent biocompatibility along with even definable bioactivity are urgently desirable for *in situ* tissue regeneration [1,2]. Although the emerging three-dimensional (3D) printing technology with remarkable developments offers a great promise to customize a personalized bioscaffold in physical structure, significant challenges in chemical and biological features of the 3D-printed bioscaffolds for the realization of individualized tissue regeneration still remain. This should be due to the limitations in terms of current biomaterials availably used as inks that dissatisfy the requirements of multi-functional tissue-engineered scaffolds. The development of bioink and the optimization of process parameters can promote the development of extrusion-based printing [3]. Application-driven inks usually require with high printing accuracy and excellent biological activity. To extensively promote the performances of current inks, exploring a universal ink modifier with outstanding dispersibility, which can easily distribute into arbitrary inks system and simultaneously endow these corresponding compound inks with enhanced characteristics to satisfy the requirements of optimized tissue regeneration, is therefore an alternative.

As far as 3D printing ink modifiers are concern, previous studies have developed a series of materials as rheological modifiers (e.g. sodium alginate [4], Pluronic F-127 [5,6], Carbomer [7], nanoclay [8–10] and nanocellulose [11]) to improve their printability, which are able to adjust the ink viscosity and rheological properties to endow the matrix ink with excellent printability to form 3D heterostructure. On this basis, for tissue engineering applications, researchers further developed a series of biological ink modifiers (e.g. β-tricalcium phosphate (β-TCP) [12,13], black phosphorus [14], graphene [15] and various active molecules [16]) to enhance the poor or unavailable biological activity of matrix inks, which can also be used in combination with rheological modifiers to develop biological active ink systems that can be directly printed [8]. However, great challenges of bioactive modifiers for 3D-printing of multi-functional tissue-engineered scaffolds still need to be improved. First, some existing active modifiers are demonstrated with special biological activity, only suitable for specific tissue repair, leading to a narrow scope of application (e.g. β-TCP and nanoclay are usually used for bone tissue engineering as active modifier [17,18]); Second, most common bioactive modifiers are nanoscale and their easy-to-aggregate properties should be one of the main obstacles in the application of 3D printing [19,20], leading to clogging of the injectors and forming the corresponding scaffolds with uneven distribution in components [21,22].

Recently, the combination of graphene materials with a material matrix as a high-performance composite biomaterial for tissue engineering has been a hot topic [23–25]. Due to their unique properties, graphene-incorporated composite biomaterials are usually demonstrated with photothermal [26], adsorptive [27], conductive [28] and shape memory properties [29] along with the enhanced mechanical properties, suggesting that graphene-based materials have the potential to be multifunctional ink modifiers. In addition, the diverse positive interactions between graphene and cells, such as promoting the differentiation of neural stem cells and adhesion of osteoblast have been confirmed, which strongly inspire the biomedical application of graphene [30,31]. However, due to van der Waals interaction, two-dimensional (2D) graphene sheets are difficult to disperse and usually trend to agglomerate in composite system, thus hindering the utilization of graphene-based composite materials. Therefore, the improvement of their dispersibility is the first emphasis for preparation of graphene-incorporated composites. Considering on its active reaction sites, nanoscale graphene oxide (nGO) with plenty of carboxylic acid and hydroxyl groups has been attracted extensive attentions [32,33]. Oxidative modification leads to more active groups, but also leads to a decrease in electrical and thermal properties [34,35]. Meanwhile, researchers have tried to improve the dispersibility of nGO by surface grafting or modification (e.g. polyethylene glycol (PEG) surface modification [36], functionalization of furfuryl alcohol [37], and grafting of poly citric acid [38]). However, these previous investigations can only increase the dispersion of nGO in limited organic solvent or only aqueous solution but be still unable to guarantee the stable and uniform distribution of nGO in the matrix material, meaning that the aggregation and settlement are still possible to happen in long-time operation process. In addition, the uneven distribution of graphene-based materials in the matrix material may also lead to the burst release of graphene during the degradation process, resulting in a dose-dependent graphene toxicity effect [39]. So far, there is no relevant research that develops a graphene-based material as an ink modifier and thus can be employed in a wide range of 3D printing processing system to fabricate multifunctional bioscaffolds with uniform distribution of graphene for tissue regeneration.

Motivated by addressing these challenges, we aim to develop an amphiphilic graphene oxide-based polyurethane (GO-PU) as an ink modifier for extrusion-based printing of multi-functional tissue-engineered scaffolds in which PEG is chosen as soft segments and nGO is used as chain extender (Scheme 1). Attributed to the amphipathic soft segment PEG, GO-PU can be prospected to disperse in various solution systems, meaning that it can be applied as an ink modifier for a wide range of 3D printing processing system. Moreover, by multipoint crosslinking between nGO and PEG, the network molecule structure of GO-PU should be formed as shown in Scheme 1, which should further benefit for the uniform distribution and long-time stable dispersion of GO-PU in other matrix materials via a physical interpenetrating manner. Due to uniform distribution of GO-PU and the matrix inks, the mechanical properties of these resulting composite materials can be significantly improved and the addition of multifunctional behaviors (e.g. photothermal, absorption capacity) should be also introduced into the corresponding 3D-printed scaffolds. In addition, the *in vitro* and *in vivo* experiments indicating that GO-PU are highly biocompatible.

2. Material and methods

2.1. Materials

PEG (number average molecular weight, M_n = 10,000 kDa), Poly (ethylene glycol) diacrylate (PEGDA, number average molecular weight, M_n = 700 kDa), Irgacure-1173, stannous octoate ($Sn(Oct)_2$), Ethylene glycol (EG), hexamethylene diisocyanate (HDI), and sodium alginate (Alg, low viscosity) were purchased from Sigma-Aldrich (California, USA). Toluene, 1,4-dioxane, dichloromethane, N,N-Dimethylformamide (DMF), tetrahydrofuran (THF), alcohol and chloroform were analytical grade and purchased from Aladdin (Shanghai, China). PLGA (number average molecular weight, M_n = 100,000 kDa) was purchased from Jinan Daigang Biomaterial Company (Shandong, China). GO was firstly purchased from Aladdin (Shanghai, China) and then treated with ultrasound and lyophilization to obtain nGO before used. Simulated body fluid (SBF) was purchased from Leagene Biotechnology (Beijing, China) and minocycline was purchased from Macklin (Shanghai, China). Modified Eagle's medium alpha (α-MEM), high glucose medium, fetal bovine serum (FBS), penicillin-treptomycin, and phosphate-buffered saline (PBS) were purchased from Gibco (USA). Trypsin-EDTA (0.25% trypsin-EDTA) was obtained from Invitrogen (California, USA).

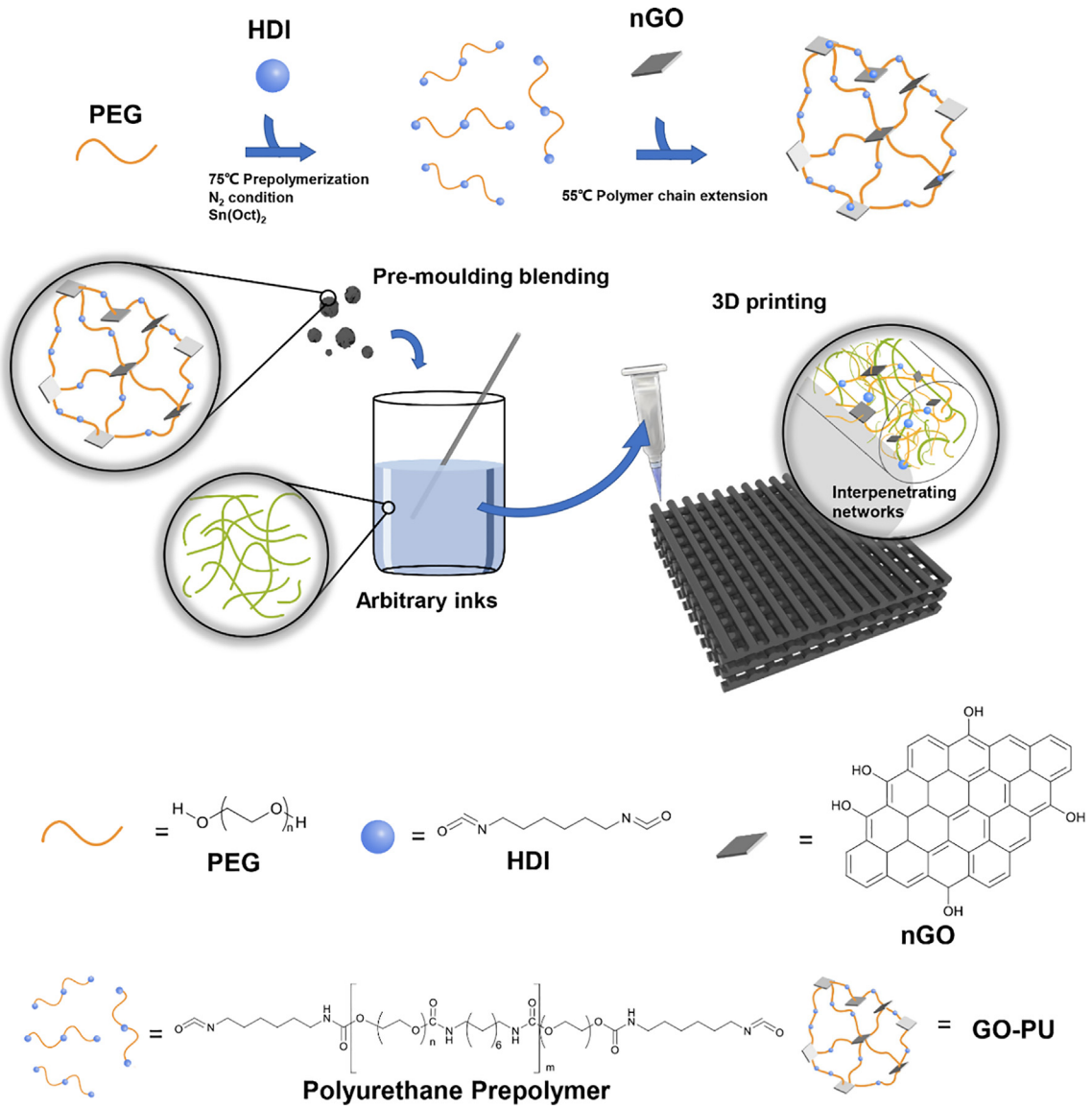

Scheme 1. A schematic diagram depicting the fabrication of the amphiphilic polyurethane ink modifier GO-PU and the application in the bioink modifcation in 3D printing. Abbreviations: PEG: Polyethylene glycol; HDI: Hexamethylene diisocyanate; nGO: Graphene oxide nanosheets.

2.2. Preparation of the amphiphilic GO-PU

The GO-PU was synthesized in accordance to our previous study [1]. In a brief, the macrodiols PEG was firstly dissolved in anhydrous toluene, then, HDI was added into the reaction system to reacting with the PEG for 3 h (the molar ratio of PEG/HDI = 1/1.2). The reaction conditions are as follows: 75 °C constant temperature, mechanical agitation, nitrogen atmosphere and Sn(Oct)$_2$ as the catalyst (Sn(Oct)$_2$/PEG = 0.75%). Subsequently, the DMF solution of nGO extender which was treated by ultrasound for 45 min advanced was added into the reactor for 8 h chain extension in 55 °C constant temperature. The GO-PUs were divided into three groups of GO-PU (0.1%), GO-PU (0.2%) and GO-PU (1.0%), which containing 0.1, 0.2, 1.0 g of nGO (the reactant PEG is 100 g), respectively. In addition, GO-PU (0.8%) and GO-PU (0.5%) also tries to use this method to synthesize. Polyethylene glycol polyurethane (PPU) was fabricated by using ethylene glycol as polyurethane chain extender instead of nGO (molar ratios of PEG/HDI/EG = 1/1.2/0.2) and PPU (0.1%) was fabricated by mixing 0.1% mass ratio of nGO into the PPU. Final GO-PU or PPU products were purified by ethanol and then collected after freeze-drying.

2.3. Polymer characterization by ^{1}H NMR and attenuated total reflection flourier transformed infrared spectroscopy (ATR-IR)

The ^{1}H NMR spectra were recorded using a Bruker spectrometer (AVANCE III 400, Bruker Inc, Massachusetts, USA), in $CDCl_3$ (TMS, 99.9+%, NMR grade, Sigma-Aldrich) solvent at room temperature and the attenuated total reflection flourier transformed infrared (ATR-IR) spectra were recorded by a Perkin Elmer spectrometer (Frontier, PerkinElmer Inc, Massachusetts, USA) in the range of 4000–600 cm^{-1}.

2.4. Morphological observation

The morphologies of the GO-PU films and fabricated scaffolds were observed by using a 3D digital microscope (RH-2000, Hirox, Japan) or a field emission scanning electron microscope (ZEISS

SUPRA 55, Zeiss, Germany). The morphologies of original and tensioned state of each sheet group should be observed. In SEM experiments, all samples were vacuum coated with platinum for 30 s before observation. Topographic characteristics of nGO were observed using an atom force microscope (AFM, MultiMode 8, Bruker, Germany).

Tensioned: at the moment when the film is stretched to break.

2.5. Transmission electron microscopy (TEM)

The presence and morphological of nGO were observed by a field emission transmission electron microscope (JEM-3200FS, JEOL, Japan). All samples were dissolved in water solution and then dropping on Copper Mesh with Ultra-thin Carbon Film to prepare the Ultra-thin samples.

2.6. Thermal analysis

The thermogravimetric analysis (TGA, METTLER TOLEDO, Switzerland) was used to characterize the thermal properties of GO-PU. The TGA tests were performed from room temperature to 600 °C at a speed of 10 °C min^{-1} and the weight changes of the samples were recorded along with the temperature increasing.

2.7. Gel permeation chromatograph (GPC)

Both number average molecular weight (M_n) and weight average molecular weight (M_w) of the GO-PU and PPU samples were measured by a GPC (Viscotek, USA) and the PDI was calculated in accordance to the formula (1):

$$PDI = M_w/M_n \quad (1)$$

Samples preparation: 2 mg/mL GO-PU or PPU dissolved in DMF, ultrasound for 25 min.

2.8. Settlement test and particle size analysis

Settlement test was used to characterize the dispersion of nGO and GO-PU in different media. 0.2 g GO-PU (0.1%) or 0.2 mg nGO was fully dispersed in 1 mL representative organic solvent or deionized water to ensure that each sample contains the same contents of nGO. Settlement situation of each sample in 2 min, 24 h and 48 h after stationary was recorded by digital camera.

Representative solvent: toluene, 1,4-dioxane, dichloromethane, N,N-dimethylformamide (DMF), tetrahydrofuran (THF), chloroform and deionized water. All solvent reagents except deionized water were analytical reagent and purchased from Aladdin.

Condition of dispersed: 25 °C Ultrasound for 15 min.

Particle size analysis: samples were dispersed in water and ultrasound for 20, 40, 80 and 120 min (concentration: 0.1%), and then the particle size were analyzed by a nano particle size analyzer (Nano-ZS instrument, Malvern, UK).

2.9. Bioink preparation

PLGA bioinks were prepared by dissolving the PLGA in 1,4-dioxane and stirring overnight. GO-PU samples with different mass ratios were added to the bioinks and fully mixed before scaffolds fabrication. PEGDA bioinks were prepared by dissolving the PEGDA in deionized water and fully dispersed. Subsequently, GO-PU and 1% Irgacure-1173 were added. Before forming for scaffolds, sodium alginate was added to the PEGDA bioinks as a molding assistant. The components of each bioink are shown in Table S1.

2.10. Mechanical analysis

PLGA bioinks with diverse GO-PU content were fabricated to membranes with size of 40 × 10 × 2 mm (length × width × thickness) by a Teflon mold for uniaxial-tensile tests. The stretching of the membranes was carried out by a universal material testing machine (INSTRON5967, INSTRON, USA) with grip-to-grip separation speed of 50 mm·min^{-1} until the membranes break.

PEGDA bioinks with diverse GO-PU content were cast into column Teflon mold and immediately fabricated to columns (d = 15 mm, h = 30 mm) by photo-initiated radical copolymerization in a XL-1000UV Crosslinker (Spectronics Corporation, NY, USA). Compression test of PEGDA was performed by a universal materials testing machine (INSTRON5967, INSTRON, USA) at a speed of 5 mm·min^{-1} until the brittle hydrogel PEGDA collapse.

2.11. Bioink rheological analysis

The rheological testing of the bioinks was carried out by a Brookfield DV-III Ultra programmable rheometer (Brookfield, USA) with spindles. Shear viscosity behaviors were determined at the shear rate of 0.01 to 100 s^{-1} in room temperature.

2.12. Scaffold design and fabrication

Scaffolds in this study were designed as cubes with the same size of 15 × 15 × 2.5 mm (length × width × height) and fabricated through cryogenic deposition 3D printing technology using a bioplotter pneumatic dispensing system (BioScaffolder 2.1, GeSiM, Germany). In a brief, the prepared bioinks were loaded into a plasticc barrel and then extruded onto a freezing stage (temperature: −40 °C) by pneumatic pump *via* a 25G (diameter: 260 μm) metal needle. The printing strands turned to solid quickly at low temperatures, neatly arranged side-by-side with 1 mm between each strand until 15 mm and deposited layer-by-layer until 2.5 mm height. The bioink extrusion pressure was set to a constant value of 75 kPa, and the translation speed of the needle was set to 5 mm·s^{-1}. Scaffold lines in adjacent layers are printed with a 90° rotation. All scaffolds were removed carefully after freezing forming and were subsequently placed in a −80 °C refrigerator (Thermo Fisher, Massachusetts, USA) for pre-freezing at least 2 h. Then, PLGA scaffolds were freeze-dried to remove the organic solvents, while the PEGDA scaffolds were crosslinking molding by photo-initiated radical copolymerization in a XL-1000UV Crosslinker. In addition, the crosslinked PEGDA scaffolds were required to be immersed in water for 6 h and washed three times to remove excess Irgacure-1173 as well as sodium alginate.

2.13. Photothermal properties and drug loading/release evaluation

A fiber-coupled continuous semiconductor diode laser (808 nm, KS-810F-8000, Kai Site Electronic Technology Co., Ltd. Shaanxi, China) was chosen as the light source. To determine the photothermal properties of the scaffolds with GO-PU molding, scaffolds with or without GO-PU were immersed in 5 mL SBF to simulated physiological environment and irradiated with a laser at a power density of 0.17 W/cm^2 for 60 s. The temperature change of the scaffolds was monitor by an infrared thermal imaging camera (Fluke TiS75, USA).

Minocycline, an antimicrobial drug, was selected as a model drug to determine the controlled release performance of scaffolds in this experiment. Scaffolds were immersed into the 1 mg/mL minocycline solution overnight for drug loading, and then gentle flushed by SBF for three times. After that, the flushed scaffolds were immersed into 5 mL SBF and static at room temperature for

controlled release experiment. At the time of 0, 1, 2, 3 and 4 h after immersed, the absorbance of 100 μL solution from each sample at 340 nm were measured using a microplate spectrophotometer (Multiskan GO, Thermo Fisher, USA) and calculate the drug concentration according to pre-determined standard curve. In addition, 60 s of near infrared radiation (NIR) stimulation at 808 nm was given at the second hour to lead to a controllable sudden release of the drug. The cumulative drug release was calculated by using the following formula (2):

$$\text{Release drug(ppm)} = \sum_{t=0}^{t} m_t \quad (2)$$

where m_t is the amount of the drug released from the scaffold at time t.

2.14. Cytotoxicity assay

L929 mouse fibroblasts were used for evaluated the acute toxicity of GO-PU (0.1%) and nGO. Cells were seeded in a 24-well plate at an initial density of 9×10^4 per well and cultured with DMEM supplemented with 10% FBS and 1% penicillin/streptomycin under a humidified atmosphere of 5% CO_2 at 37 °C for 24 h incubation. Materials were sterilized and re-suspended into fresh culture medium to obtain the required concentration of suspension. After incubating the plate at 37 °C under a humidified atmosphere of 5% CO_2 for 5 h, the suspension in each well was replaced with the fresh cell culture medium. The CCK-8 testing (CCK-8, Dojindo, Kumamoto, Japan) was performed after 24 h of post treatment incubation for determine the cell viability (%) in each well in accordance to the manufacturer's instructions. Wells without any material supplemented were considered as the control group. Live/Dead imaging (Live or Dead™ Cell Viability Assay Kit, ATT Bioquest, USA) was also carried out for observed the cell morphology at the same time. All measurements were repeated three times. 3T3 mouse fibroblasts were used as an alternative cell for the same experiment to ensure that the results were credible.

2.15. In vivo evaluation of the biocompatibility and toxicity of GO-PU bioink.

8-week-old female Balb/c mice were purchased from Charles River Co. Ltd. (Beijing, PR China), and were housed in specific pathogen free environment. They were given free access to water and a normal commercial laboratory diet. After a week of environmental adaptation, the mice were randomly divided into three groups of 10 each. To determine the administered dose, we calculated that the GO-PU contained in one scaffold (15 × 15 × 2.5 mm) was 1.3 mg, hence we defined 1.3 mg GO-PU/mice as a "low dose" and 13 mg GO-PU/mice as "high-dose". The experimental groups were divided into control group (0.9% Nacl), low-dose group and high-dose group according to the injection dose. The day of the subcutaneous injection was designated as the 0 day. The procedure was pre-approved by the Ethical Committee of the Shenzhen Institutes of Advanced Technology, CAS (SIAT-IACUC-190730-YYS- YJR-A0874). Mice were sacrificed on 3rd day and 7th day after the injected procedure for histological analysis of the skin, heart, liver, spleen, lung and kidney. For biochemical analysis, the blood and the serum were collected on the 7th day (4 mice were sacrificed for blood collecting and another 4 mice were sacrificed for serum collecting). Briefly, a full-thickness skin sample with a 1 cm margin around the injected area was removed from each animal, and was fixed in 4% (v/v) paraformaldehyde in PBS overnight. The tissue sample was embedded in paraffin after dehydration, sectioned at 3–4 μm, and stained with hematoxylin and eosin (H&E) or Masson's trichrome. The stained sections were observed and photographed under a microscope (Leica, Germany). Similarly, the heart, liver, spleen, lung and kidney of the mice were collected and treated in the same way. The blood and serum samples were analyzed by the Automated whole cell hematology analyzer (BC-2800vet, Mindray, China) and the Automatic biochemical analyzer (Chemray-240, Rayto, China).

2.16. Statistical analysis

At least four parallel samples ($n \geq 4$) were performed in all experiments which required statistical analysis. All data were expressed as means ± SD and processed with Graphpad Prism 7 or OrginPro 8 software. The *t*-test was used for the mean differences between two groups or ANOVA was used if more than two groups were involved. *, $P < 0.05$. **, $P < 0.01$. ns, no significant difference.

3. Results and discussion

3.1. Preparation and characterization of the amphiphilic GO-PUs

As shown in Scheme 1, GO-PUs were prepared with the amphiphilic PEG as soft segment while hexamethylene diisocyanate (HDI) and nGO as chain extenders according to a two-step method. Before adding to the reactor, nGO was fully dispersed in DMF by ultrasonic treatment for 15 min to ensure that it was uniform and single-layered with about 2–4 nm thick, which were determined by AFM (**Figure S1**). By regulating the mass ratio of nGO/PEG from 0.1/100, 0.2/100 to 1.0/100, GO-PUs with a gradient content of nGO were successfully obtained and coded as GO-PU (0.1%), GO-PU (0.2%) and GO-PU (1.0%), respectively. Besides, the polymer of ethylene glycol (EG)-based polyurethane (PPU) obtained by only using EG instead of nGO as extender and the composite by physical mixture of PPU and 0.1% nGO (mass ratio of nGO/PPU = 0.1/100, coded as PPU (0.1%)) were chosen as the control, respectively. The ^{1}H NMR (**Figure S2**) and ATR-IR (**Figure S3**) measurements verified the successful preparation of GO-PU. In **Figure S2**, the peaks between 1 and 1.5 ppm, the peaks at about 3.2 ppm and the peaks at about 4.2 ppm of all groups were assigned to —CH_2—, —NH—CH_2— and isocyanate bonds of HDI, respectively [40]. Moreover, comparing with PPU, a sharp peak near 1.8 ppm was observed in GO-PU, while only a blunt peak at the similar chemical shift was observed in PPU (0.1%). This may be attributed to the difference of active hydrogen between nGO in GO-PU (0.1%) by chemically grafting and nGO in PPU (0.1%) by physical blending, suggesting the successful introduction of nGO into polymers but with different methods. Further, as shown in **Figure S3**, in the ATR-IR spectra of GO-PUs and PPU, the absorption band of —N=C=O at 2350 cm^{-1} was invisible while the absorption bands at 1528 cm^{-1} and 1720 cm^{-1} corresponded to the C=O and amide II respectively were visible, indicating the successful reaction between isocyanate and —OH and the formation of carbamate bonds [40]. In addition, a weak absorption bend could be observed at 1655 cm^{-1} in only GO-PU samples, which should be attributed to the stretching vibration of C=C bond in nGO [41]. With the increase of nGO contents, the absorption bands tended to be stronger.

To further clarify the properties of GO-PU, GPC and TGA characterizations were performed. As summarized in **Figure S4A**, GPC results also showed that polymer dispersity index (PDI) tended to decrease with the increase of nGO, indicating that molecular structure of GO-PU were preferring to form straight chain rather than network chain while increasing the nGO extender (**Figure S4B**). Due to the steric hindrance, when the nGO is lacked, the hydroxyl groups on the same graphene can be reacted by more

macromolecular alcohols, thus forming a tangled network structure; when there is more graphene added, the macromolecular alcohols tend to react with free nGO sheets. Besides, the molecular weight of straight-chain GO-PU (1.0%) was higher than those of network-chain GO-PU (0.1%) and GO-PU (0.2%). Two obvious thermal decomposed stages could be easily observed in the TGA curves of the GO-PUs and PPU (0.1%) but only one decomposed stage in pure PPU (**Figure S5A**), suggesting that the first stage around 270 °C should attribute to the oxidative decomposition of nGO and the second stage around 400 °C should attribute to the decomposition of PEG segments in polyurethane. In particular, the initial temperature (T_{Ini}) and the maximum temperature (T_{Max}) of the first stage and the ash% of all groups were recorded in **Figure S5A**. It was found that both T_{Ini} and T_{Max} of the oxidative decomposition of chemically grafted nGO in GO-PU groups were higher than those of physically mixed nGO in PPU (1%), indicating that the chemically grafted nGO in GO-PUs is able to tolerate higher temperatures. This was because pure nGO directly turned to carbon oxides and escaped into the air at a certain temperature, while the nGO in GO-PU, which combined with polyurethane through carbamate bonds, had to break the carbamate chemical bond by consuming some of the internal energy prior to be oxidized (**Figure S5B**). Meanwhile, it was noteworthy that the oxidation decomposition temperature of nGO in GO-PU (1%) was lower than those of nGO in GO-PU (0.1%) and GO-PU (0.2%), due to the difference of entanglement combination of PEG chains and nGO between the liner polymer chains of GO-PU (1%) and network polymer chains of GO-PU (0.1%) and GO-PU (0.2%) (**Figure S5B**), which was accorded with the results from GPC.

Next, the mechanical properties of GO-PU (0.1%, 0.2% and 1%), PPU and PPU (0.1%) were further evaluated. PPU (0.1%) is a control group that the PEG-based polyurethane with the physical mixture of 0.1% nGO. As shown in Fig. 1**A,** GO-PUs showed better mechanical properties than PPU groups in generally. Both tensile stress and elongation at break, GO-PU groups were significantly better than PPU groups. This might be attributed to the existence of main block segments between PEG soft segments and nGO layers to hence form a network structure in GO-PUs (Fig. 1**B**). The interfacial interaction between graphene and materials is helpful to improve the mechanical properties of materials therefore was without any surprise that the addition of nGO could improve Young's modulus of PPU (Fig. 1**C**). Similar with the PPU, the increase of nGO contents was able to improve Young's modulus of GO-PU, which might be the explanation of the phenomenon that Young's modulus of GO-PU (0.2%) was better than GO-PU (0.1%) (Fig. 1**C**). However, the Young's modulus of GO-PU (1%) was significantly lower than GO-PU (0.2%), which might be attributed to the difference in molecular structure (**Figure S4**). The tensile stress of GO-PU (0.1%) could even reach 10 MPa (Fig. 1**D**), and its elongation at break neared 400% (Fig. 1**E**) This is attributed to the unique micro network structure of GO-PU, which can effectively resist external force tearing, thus showing stronger tensile stress than linear polyurethane PPU. Meanwhile, the tensile stress and elongation at break of PPU (0.1%) were slightly higher than those of PPU, which might be due to the weak hydrogen bonding force between the nGO and PEG (Fig. 1**A, D and E**).Further, the stretch evaluation of GO-PU (0.1%) directly demonstrated its good toughness (Fig. 1**F**) and the variation of surface morphologies of GO-PU (0.1%) and PPU film were explored by 3D digital microscope and SEM. As shown in Fig. 1**G**, GO-PU film showed a relatively uniform black color and with uniform black particles distributed under 3D digital microscope in the original state, while PPU film performed as pure white. The network fibers on the surface of GO-PU could be observed under SEM, while the fibers on the surface of PPU were not obvious. The stretched fibers of GO-PU could be seen under 3D Digital Microscope (Fig. 1**G**) and SEM (Fig. 1**H**); on the contrary, due to the poor toughness of PPU, it could hardly be stretched and only a few stretched fibers could be captured on the fracture surface under 3D digital microscope while almost no fibers could be seen under SEM (Fig. 1**G**). Meanwhile, a large amount of nGO should be seen like linkers between the stretched GO-PU fibers under SEM (Fig. 1**G**), which endowed excellent toughness to the polyurethane through chemically bonded (Fig. 1**B**).

It was found that the mechanical properties of GO-PU tend to decline with the graphene content increasing. We also tried to synthesis the GO-PU (0.08%) and GO-PU (0.05%) for higher PDI, however, the mechanical properties of GO-PU (0.08%) had shown no significant different with that of GO-PU (0.1%), and the synthesis of GO-PU (0.05%) even failed (**Figure S6**). Besides, the productivity of GO-PU (0.08%) was significantly lower than the GO-PU (0.1%). As consequences of the network GO-PU with more excellent mechanical properties and simultaneous introduction of nGO as much as possible, the follow-up experiments were carried out with GO-PU (0.1%).

3.2. Excellent dispersity and printability of GO-PU

One of the primary indicators of a universal ink modifier is to be able to uniformly mix in a variety of solution processing systems, and to maintain stable for enough time for mass production. As shown in Fig. 2**A**, GO-PU could be stably dispersed in organic solvents or aqueous system at different concentrations. As the concentration increased, the viscosity also showed an upward trend (Fig. 2**B**), benefiting for extrusion printing process. We also observed the viscosity of GO-PUs with different content of nGO, and the results showed that when the content of nGO increased, the viscosity tends to be decreased (**Figure S7**). Further, as shown in Fig. 2 (**C and D**), the dispersity and stability of GO-PU and pure nGO with the equal concentration of 0.2 mg/mL nGO in seven representative system were detected. It was as expected that GO-PU could be evenly dispersed in organic or aqueous solution for at least 24 h (Fig. 2**C**), while pure nGO obviously precipitated in the dispersed phase except DMF and water (iii and vii) only 2 min after ultrasonic dispersion (Fig. 2**D**); with the extension of time to 48 h, partial precipitation could be seen at the bottom of the bottle of GO-PU groups. In contrast, nGO with the same contents could only maintain a certain degree of dispersion in DMF (iii) and water (vii) for only 24 h after ultrasound (Fig. 2**B**), indicating that its dispersity is far less than GO-PU. This may be attributed to when GO-PU enters the solution system, the amphiphilic PEG soft segments open a large "cage" in the solution while nGO enters the solution system, the strong van der Waals interaction makes it easy to aggregate and settle (Fig. 2**E**); The "cage" efficient prevents the van der Waals interaction on the surface of nGO, thus preventing the occurrence of aggregation and settlement. In order to confirm our conjecture, we used particle size analyzer to analyze the swelling of GO-PU and PPU in aqueous solution. According to the previous section of structure characterization, with the increase of nGO content, GO-PU will be closer to the linear structure, which is not conducive to the formation of "cage" structure, resulting in smaller swelling and smaller particle size. As shown in **Figure S8**, we observed that GO-PU had more obvious swelling behavior and larger particle size than PPU, and this phenomenon tended to disappear with the increase of nGO content. This is consistent with our structural characterization and speculation. Relevant analysis instructions can be seen in the description of **Figure S8** in supporting information.

Further observation and comparison of the nGO states in GO-PUs and PPU (0.1%) were essential for further confirmation of this view, and therefore the TEM image of pure nGO, PPU (0.1%), and GO-PUs were taken and be analyzed (**Figure S9**). TEM results showed that the pure nGO was relatively transparent and not easy

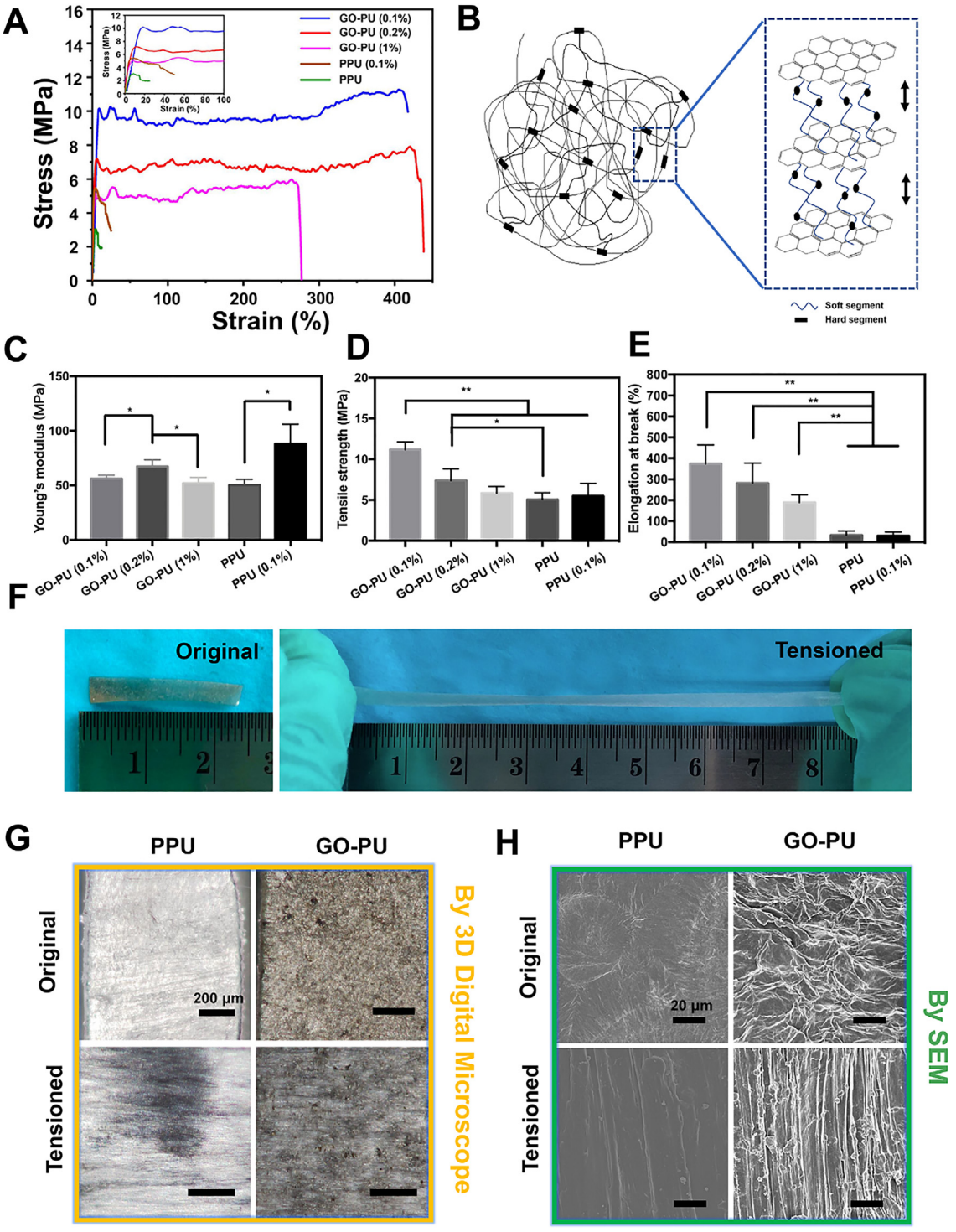

Fig. 1. (A) Stress–strain curves of GO-PUs and PPUs. (B) Network structure between each nGO in GO-PU. (C) Young's modulus of GO-PUs and PPUs. (D) Tensile strength of GO-PUs and PPUs. (E) Elongation break (%) of GO-PUs and PPUs. (F) Strong toughness of GO-PU (0.1%). (G) and (H): Surface morphologies of GO-PU membranes observed by 3D Digital Microscope (G, with scale bar of 200 μm) and SEM (H, with scale bar of 10 μm). Statistical significance was set to $^{**}p < 0.01$ and $^{*}p < 0.05$.

to fold (**Figure S9 A, E and I**); and the binding sites of PEG and nGO in PPU were disordered, irregular and accumulated in a large area, while in GO-PUs there were various uniform dots, which indicated that the bonding modes of PEG and GO on graphene surface were different (**Figure S9B, F and J**). In all samples, the parallel lattice planes had been observed (**Figure S8**). The planes showed an ordered stacking with the interlayer spacing of 0.33 nm (**Figure S9C, G and K**). In **Figure S9D**, the diffraction spots were comparatively diffuse and show constant intensity. This implies that the nGO sample used comprises free sheets that have not aligned in a way that makes them exactly perpendicular to the incident electron beam. After mixing with PU or after PU conjugation, no lattice fringing had been observed, but a more diffuse halo ring was formed. This showed that the degree of crystallinity was further declined because of the PEG coating (**Figure S9H**). Compared to the case of mixing of PPU (0.1%), the decline in the degree of

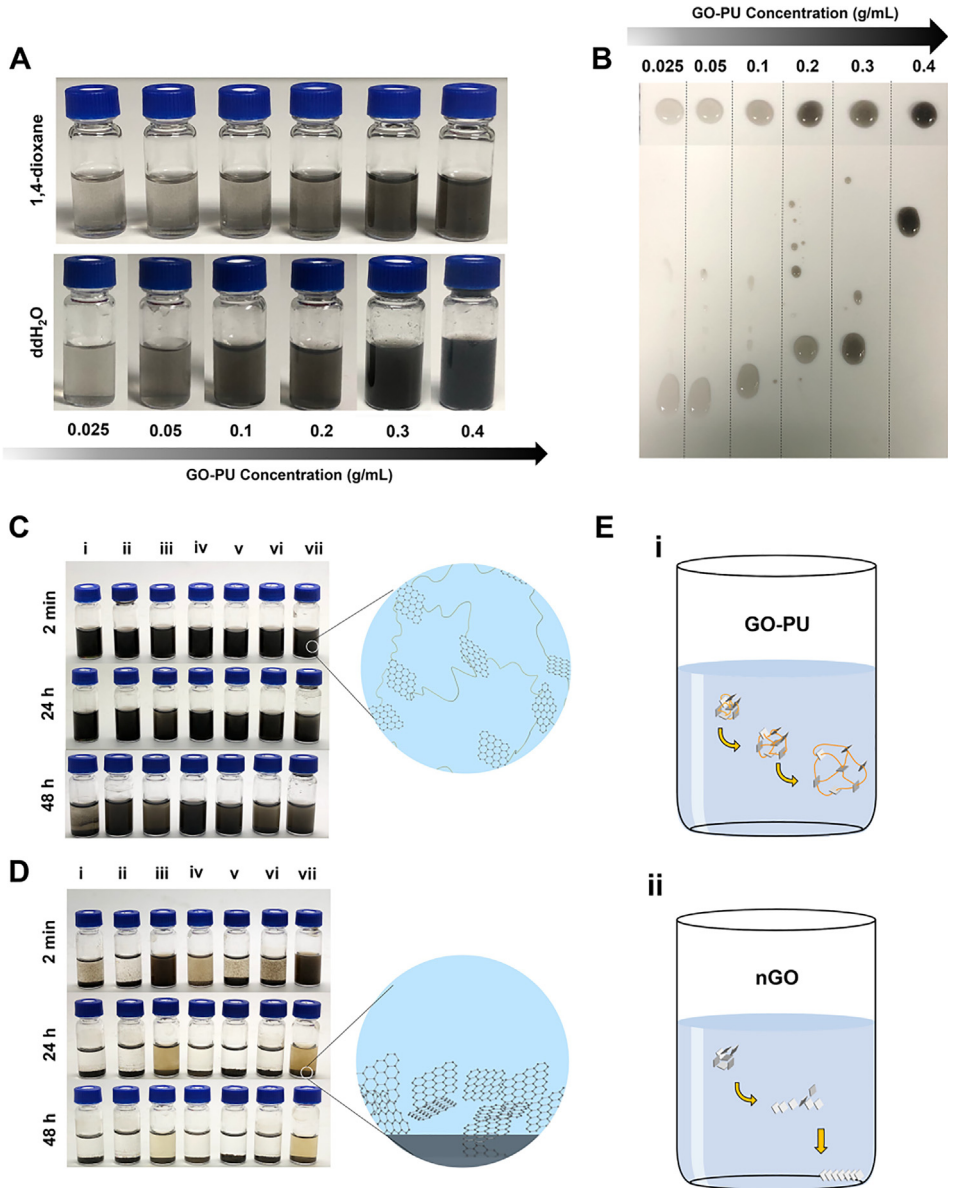

Fig. 2. (A) Different concentration of GO-PU can be evenly dispersed in water and organic solutions. (B) The viscosity of GO-PU dispersion increases with concentration; dissolvant: ddH2O; background: teflon; flowing Time: 5 s. (C) and (D) GO-PU (C) and nGO (D) settlement situation of 2 min, 24 h and 48 h after setting in diverse solvents of (i) toluene; (ii) 1,4-dioxane; (iii) N,N-dimethylformamide (DMF); (iv) dichloromethane; (v) chloroform; (vi) tetrahydrofuran (THF); (vii) deionized water. (E) Schematics diagrams depicting the behavior of GO-PU (i) and nGO (ii) as they enter the solvents.

crystallinity was more significant for the case of GO-PU, indicating that the uniform PEG layer hinders the observation of crystallinity of nGO. (**Figure S9L**). In summary, the PEG segments between nGO in GO-PUs leads to the increase of steric hindrance between nGO sheets, which, together with the decrease of crystallinity, may contribute to the increase of dispersion.

In extrusion-based printing, a large amount of deposition and aggregation of the materials should lead to uneven distribution of the materials in the matrix, and even lead to blockage of needles, further limiting its application. As the excellent dispersity, anti-aggregation and suitable viscosity of GO-PU, it should be a great potential to be directly applied as an ink to fabricate 3D graphene-based devices. In the previous studies, although a few graphene-based devices had been fabricated under very severe printing conditions, this kind of graphene-base ink that could be suitable for various 3D-printed processing systems has not been reported yet [42–44]. Due to the suitable viscosity with proper concentration of GO-PU, it was capable for 3D printing by layer stacking to prepare 3D graphene devices, and its fiber diameter could reach 200 μm (**Figure S10A and B**). It was found by the SEM observation that the surface of the scaffold prepared by pure GO-PU had certain pores, and no obvious aggregation found (**Figure S10C**). That is to say, GO-PU ink can be printed with high precision, showing a potential to fabricate customized 3D graphene devices. However, attributed to the dispersity of GO-PU in numerous solutions, the fabricated 3D graphene devices cannot stably keep the structure when they meet in water-based or organic-based solution, further limiting its application for directly printing of pure GO-PU devices. Therefore, all of these evidences encourage us to further explore GO-PU as the ink modifiers to fabricate multi-functional scaffolds with excellent performances resulted from incorporation of nGO.

3.3. GO-PU as the ideal ink modifiers

In order to thoroughly evaluate the improvement of inks by adding the GO-PU ink modifier, solvent-phase processing bioink PLGA and water-phase processing bioink PEGDA were used as the representative inks. PLGA is a FDA-approved biomedical material that is considered an ideal material for tissue engineered bone repair because of its mechanical properties, biocompatibility, and ease of processing [45]. PEGDA is a PEG derivative with double bond, which can be cured by UV initiation under initiator conditions to form a solid with adjustable mechanical properties [46]. However, both PLGA and PEGDA usually lack biological activity and intelligent response, thus limiting their utilization in 3D printing of tissue regenerative scaffolds [47]. For ink modifier, the effect of its addition amount on the matrix material should not be ignored. Too low concentration of modifier may not enough to endow the function to the matrix materials, while the too high concentration may affect the biological properties (e.g. the toxicity from the modifier may cause the decline of biocompatibility of matrix) or forming process of the matrix material (e.g. the modifier affect the crosslinking efficiency of light-induced ink). As far as ink modifier concerns, the amount is usually less than 10 wt% in the matrix [6,8]. Therefore, we will use the addition amount of 2.5%, 5%, 7.5% (wt% of liquid bioink PEGDA and ww% of solid bioink PLGA) GO-PU as the experimental group for the following experiment.

3.3.1. GO-PU significantly enhances the mechanical properties of its composite materials

We successfully prepared the composite samples for mechanical test by mixing PLGA or PEGDA with GO-PU, the results were as shown in Fig. 3**A** and their detailed compositions were depicted in **Table S1**. In particular, the uniform PLGA/GO-PU composite films were obtained by molding the PLGA/GO-PU composite solution (1,4-dioxane as the solvent) and subsequently lyophilizing. The PEGDA composite columns were fabricated by adding initiator-1173 to PEGDA/GO-PU solution and further treated with UV irradiation in a column mould. As brittle materials, the mechanical properties of PEGDA were determined by compression; on contrast, as ductile materials, we used tensile to determine its mechanical properties of PLGA. As shown in Fig. 3 **(B and C1)**, the compressive strengths of PEGDA (5 %GO-PU) and PEGDA (7.5 %GO-PU) were significantly higher than those of pure PEGDA and PEGDA (2.5 %GO-PU). There was no significant difference in the compressive strain at break of all groups (Fig. 3**C2**). The varied trend of compressive modulus of PEGDA material after introducing GO-PU was consistent with that of compressive strength; the introduction of 5% and 7.5% GO-PU could significantly enhance the compressive modulus of PEGDA, while the improvement of composites materials by introduction of 2.5% GO-PU was no significant comparing with pure PEGDA (Fig. 3**C3**). It is worth noting that PEGDA (7.5% GO-PU) has no significant increase compared with PEGDA (5% GO-PU) in both compressive strength and compressive strength at break, which may due to the inadequate crosslinking of PEGDA (7.5% GO-PU) (**Figure S11A**). In **Figure S11A**, we further discussed the effects of the addition amounts of GO-PU on the process of photoinitiated radical polymerization by a flat-leaned method and when the addition amounts of GO-PU were up to 7.5%, the inadequate crosslinking of PEGDA was observed after 60 s. For PLGA, the addition of GO-PU could significantly increase the tensile strength and tensile modulus. The tensile strength of PLGA (2.5% GO-PU), PLGA (5% GO-PU) and PLGA (7.5% GO-PU) was significantly higher than that of PLGA group (Fig. 3**D, E1 and E2**). Similar to the change of tensile stress, the introduction of different content of GO-PU could also significantly improve the tensile modulus of PLGA, especially when the amount of GO-PU introduced was 5% (Fig. 3**E3**). However, the tensile modulus of PLGA (7.5% GO-PU) showed not statistical difference to the PLGA group. Consequently, it can be concluded that the 5% addition amount of GO-PU are suitable for both ductile materials and brittle materials for future application. An interpretation for the enhancement on mechanical properties of composites by introduction of GO-PU ink modifier is that the polymer chains from matrix materials can insert into the GO-PU network to form a dual network structure (**Figure S11B**). According to mechanical tests, when the GO-PU content is 5%, the composite material has relatively best performance, suggesting the optimal dual network to be formed. In the samples that contain 7.5% GO-PU, excessive GO-PU addition can't be fully interlaced into the dual network structure, resulting in no significant difference on the enhanced mechanical property.

3.3.2. GO-PU endows multifunctional performances of 3D-printed GO-PU based scaffolds

Further, we used the GO-PU as ink modifier with the addition amount of 5% to successfully fabricate complex GO-PU based scaffolds with three typical inks including PLGA, PEGDA and alginate, as shown in Fig. 4**A** and **Figure S12**. There was no needle blockage throughout the 3D printing process and the bioink with 5% GO-PU added was slightly black and the printed scaffold was uniform in color (Fig. 4**B**). For the brittle material PEGDA, the scaffolds prepared with GO-PU adding exhibited more ductile **(**Fig. 4**C)**. We performed rheological tests on PLGA and PEGDA bioinks with or without the addition of GO-PU and found that bioinks with 5% GO-PU showed a more pronounce shear thinning, indicating that the composite bioinks exhibited better printability in extrusion printing process **(**Fig. 4**D, E)**. The rheological properties show that it can realize scaffolds printing with complex or special structure such as gradient printing scaffolds, so as to further enhance the mechanical properties **(Figure S12)** [48]. In addition, due to the introduction of functionalized nGO, the matrix materials were endowed with some additional properties that were not originally possessed, such as photothermal properties. By 808 nm NIR (Near Infrared Radiation), scaffolds containing GO-PU emitted heat for functional application of the matrix material. As shown in Fig. 4**F**, minocycline, a drug with a pale-yellow appearance was used as a model drug to demonstrate that GO-PU endowed PEGDA and PLGA with controlled release ability. Due to physical adsorption, nGO in GO-PU were able to adsorb the drug in the solution, and the adsorbed drug were controllably released due to the increase of Brownian motion when triggered through 808 nm NIR. As shown in Fig. 4**G**, the PLGA (5% GO-PU) scaffold rose from room temperature to 47.7 °C by 808 nm NIR for 1 min, while the PLGA scaffold only rose to 28.2 °C; the PEGDA (5% GO-PU) scaffold rose to 56.3 °C, while the PEGDA scaffold only rose to 30.7 °C. The heating curves are shown in **Figure S13.** This indicates that the introduction of GO-PU endows the matrix materials of PLGA or PEGDA with a significant photothermal effect. For the hydrophobic polymer PLGA, it is difficult to preserve the drug by absorbing the drug solution so that it is difficult to achieve the drug-loading effect, however, the modifier GO-PU endows a drug-loading function thereto. The drug minocycline in the solution was physically adsorbed to the surface of the scaffolds containing GO-PU, so that the scaffolds appeared to be pale yellow, while the scaffolds without GO-PU were not able to adsorb the drug, and the appears of scaffolds were no change after overnight immerse into the drug solution (Fig. 4**H)**. When stimulated by NIR at 808 nm, the scaffold containing GO-PU could release the drug and turned the

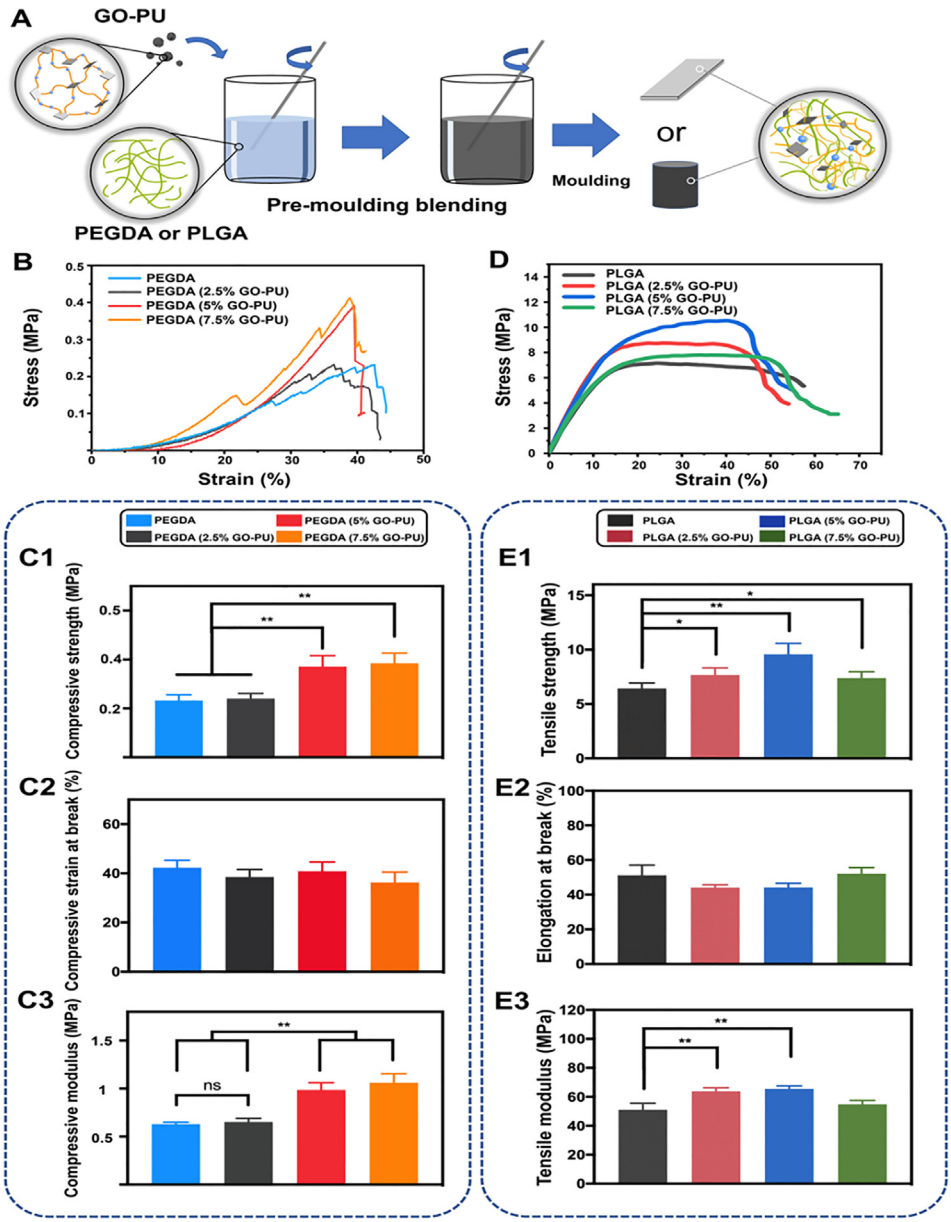

Fig. 3. (A) A schematic diagram depicting the composite materials formed of GO-PU and matrix materials. (B) Stress–strain curve, (C) compressive strength, compressive strain at break and compressive modulus of PEGDA cylinders with different contents of GO-PU in the compression test. (D) Stress–strain curves, (E) tensile strength, elongation at break and tensile modulus of PLGA membranes with different contents of GO-PU in the tensile test. All of the statistical significances were set to $^{**}p < 0.01$ and $^{*}p < 0.05$.

original colorless solution to light yellow (Fig. 4**H**). The light-triggered drug release of these obtained scaffolds was further quantified. All scaffolds were previously immersed in the same concentration of minocycline solution overnight for drug loading and then were simulated the drug release process in SBF. Because PEGDA hydrogel scaffolds could absorb a lot of water, there was no significant difference in the drug release amount of PEGDA scaffolds with or without GO-PU at first hour (Fig. 4**I**). However, when the NIR was performed at the second hour, it was found that the PEGDA scaffolds containing GO-PU showed a sudden release of the drug, while the scaffolds without NIR or the scaffold without GO-PU showed no drug burst (Fig. 4**I**). The pure hydrophobic PLGA scaffolds were almost impossible to carry the drug and there was almost no drug release whether the NIR was performed or not at the second hour; the PLGA scaffolds containing GO-PU were able to load drug by physical absorption so that it was able to slowly release the drug due to the diffusion effect (Fig. 4**J**). More importantly, at the second hour, the amount of drug released in the PLGA (5% GO-PU) + NIR groups was significantly higher than that of the group without NIR but containing GO-PU (PLGA + GO-PU). These evidences indicate that GO-PU can promote physical adsorption of the drug and can be controlled release by NIR at 808 nm. Therefore, the introduction of GO-PU can improve the mechanical properties and printability of the bioinks and meanwhile endows multi-functional properties of the resulting scaffolds from the incorporated functional nGO segments, such as photothermal controlled release. This

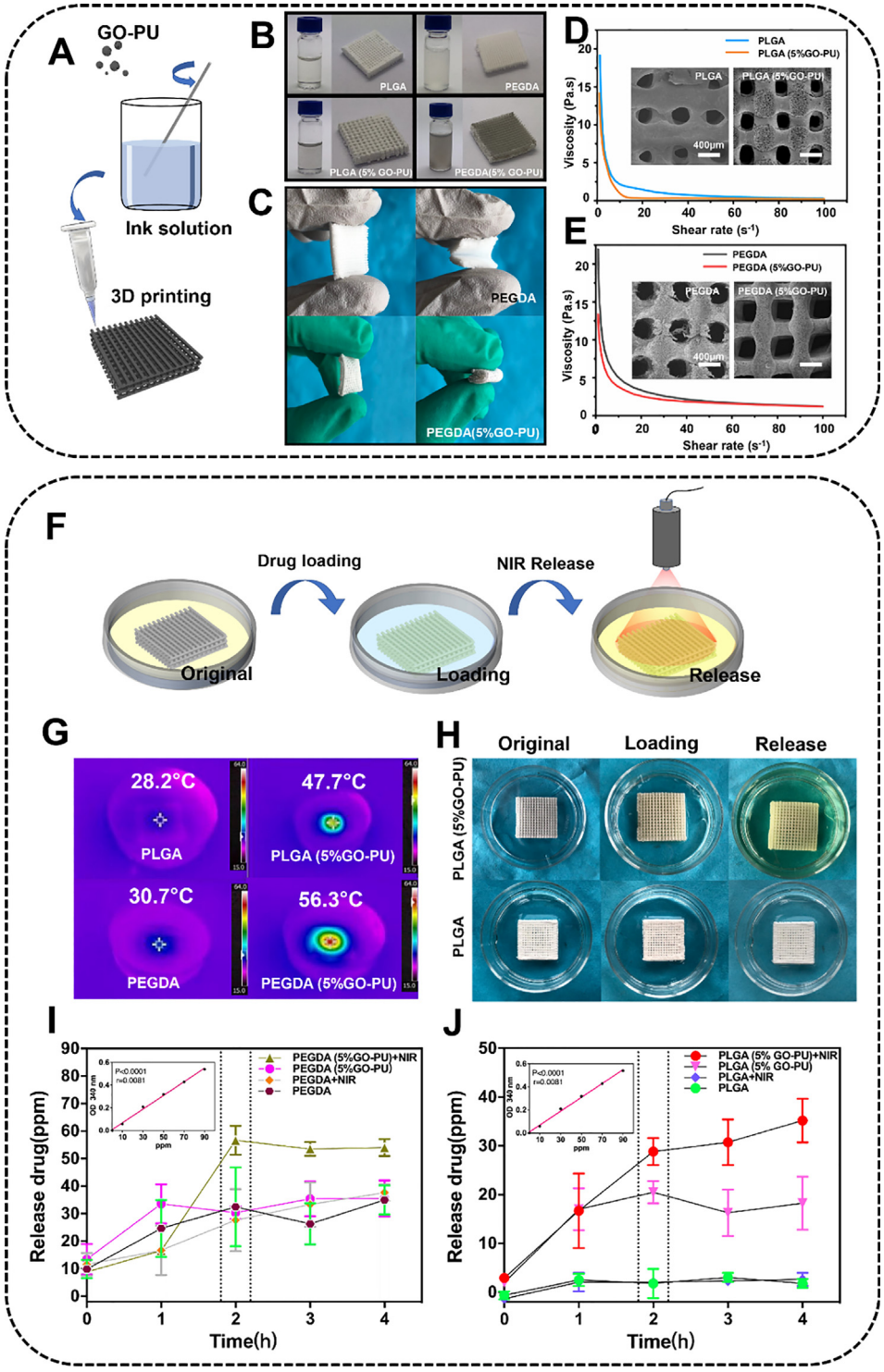

Fig. 4. (A) A schematic diagram depicting the composite scaffolds formed of GO-PU and matrix bioinks. (B) Bioinks and scaffolds of PLGA or PEGDA with or without GO-PU containing. (C) PEGDA scaffolds with or without GO-PU were bent at several angles; scaffolds in the gray glove: PEGDA, scaffolds in the green glove: PEGDA (5 %GO-PU). (D) and (E) Changes in the viscosity of PLGA (D) or PEGDA (E) bioinks with or without GO-PU from 0.1 to 100 rad s^{-1} and the morphologies of PLGA (D, inside) or PEGDA (E, inside) scaffolds with or without GO-PU. (F) A schematic diagram depicting photothermal controlled release of drug-loading scaffolds. (G) Photothermal performance of scaffolds irradiated by the 808 nm laser for 1 min (0.17 W/cm^2) with or without GO-PU. (H) The original (left), drug loading for overnight (middle) and photothermal release (right) situation of PLGA (upper) and PLGA (5 %GO-PU) (bottom) scaffolds. (I) and (J) Cumulative release curve of PLGA (I) and PEGDA (J) scaffolds with or without GO-PU, and with or without NIR. The scaffolds irradiated by the 808 nm laser for 1 min at the 2nd hour. (For interpretation of the references to color in this figure legend, the reader is referred to the web version of this article.)

characteristic may inspire researchers to develop intelligent bioink for tissue engineering or drug delivery by using matrix materials and GO-PU.

Although nGO can physically disperse into the material system by a series of means such as ultrasound, it may not be stable and should precipitate into the medium due to the water exchange. The introduction of nGO by adding GO-PU into the matrix should provide an effective alternative to improve its stability in the GO-based materials. As shown in **Figure S14A1**, when pure nGO was homogeneous mixed into the matrix by ultrasound, the material presented yellow brown color, and the distribution of the nGO in the matrix material was not uniform. After immersion in SBF for 3 days, nGO precipitation was observed (**Figure S14A2**). In contrast, the as-prepared composite PEGDA/GO-PU without photocrosslinking appeared light black, showing a uniform, non-aggregated morphology **(Figure S14B1 and B2)**. After further photocrosslinking, the appearance of the composite PEGDA/GO-PU material transformed to a uniform brownish black color, due to the formation of rigorous polymer network structure **(Figure S14C1)**. Meanwhile, nGO particles could not be seen on the surface of composite PEGDA/GO-PU material, and no nGO precipitated when it was immersed in SBF after 3 days **(Figure S14C2)**. This phenomenon could also be observed in the 3D-printed scaffolds after adding GO-PU. No nGO particles precipitated from the scaffolds immersed in the solution on day 0 **(Figure S14D)** and day 3 **(Figure S14E)**, and no difference was observed compared with the pure PEGDA scaffolds **(Figure S14F)**. That is to say, GO-PU can uniformly and stably distribute in the arbitrary ink materials through forming the dual network structure between ink materials and GO-PU, thus enhancing the properties of the resulting composite inks without any participation of chemical reactions.

3.4. GO-PU has excellent biocompatibility

In section 2.15, we calculated that the GO-PU contained in one scaffold (15 × 15 × 2.5 mm) was 1.3 mg which nGO equivalent is 0.0013 mg. The body fluids of mammals account for about 60% of the body weight, according to the conversion, after implantation of a scaffold, the content of nGO in the mice (16–20 g weight) body fluid was increased to about 0.1 mg/L. Since the toxicity of graphene is dose-dependent, we believe that such a low content will not cause cytotoxicity. In order to verify this, we carried out the corresponding cell experiment. As shown in Fig. 5**A and B**, the results of Live/Dead imaging and CCK-8 showed that GO-PU had high biocompatibility. With the increase of the dose, the L929 cell morphology and survival rate did not change significantly. For further verification, 3 T3 fibroblasts were also used to repeat the viability experiment, and the results were consistent with the conclusion of L929 group **(Figure S15)**. The results of cytoskeleton staining showed that the cells could adhere to the scaffolds with excellent morphology whether GO-PU was added or not **(Figure S16)**. In order to further demonstrate the biocompatibility of GO-PU in vivo, we injected GO-PU into mice subcutaneously. Histological staining on the third and seventh days after injection showed that neither low-dose nor high-dose GO-PU caused inflammatory infiltration (Fig. 5**C**). The skin tissue and collagen layer were intact in all groups (Fig. 5**C**). These results indicate that GO-PU has excellent biocompatibility when contacting tissues and cells and does not cause contact toxicity, indicating its great potential for applications in tissue engineering. Due to the excellent dispersion of GO-PU, we did not observe the deposition of GO-PU in the subcutaneous tissue of the injection site on the third and seventh day, therefore, we did toxicological tests on the seventh day to characterize the biocompatibility of GO-PU.

To further verify the biocompatibility performance of GO-PU in vivo, we collected blood and serum from the mice on the seventh day after subcutaneous injection of GO-PU for biochemical characterization. The white blood cells (WBC), red blood cells (RBC), mean corpuscular volume (MCV), platelets (PLT), mean corpuscular haemoglobin (MCH), haemoglobin (HGB), haematocrit (HCT), and mean corpuscular haemoglobin concentration (MCHC) were measured (Fig. 6**A**). The results showed no significant difference compared with the control group for either low or high doses of GO-PU, revealing that GO-PU does not exert deleterious effects. Blood biochemical examination was also carried out and the biochemical parameters including alanine transaminase (ALT), aspartate transaminase

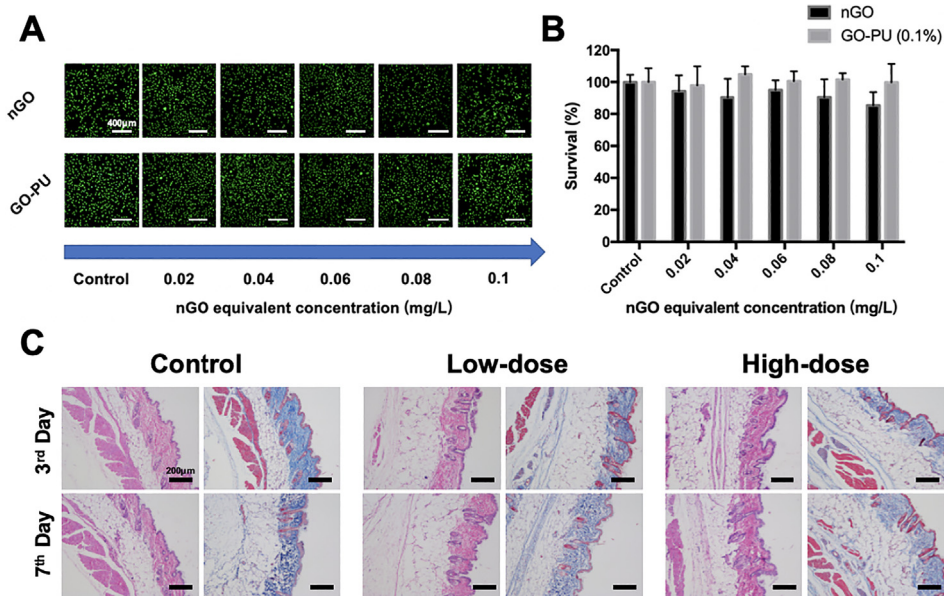

Fig. 5. (A) Live (green)/Dead (red) fluorescent images of L929 cells treatment with different concentration of nGO or GO-PU, after 24 h of post-treatment incubation. (B) Viability of L929 after treatment with nGO and GO-PU (0.1%), after 24 h of post-treatment incubation; (C) Histological analysis of the injection site on 3rd day and 7th day after injection. Sections of the injection site are stained with H&E and Masson's trichrome. All of the statistical significances were set to $^{**}p < 0.01$ and $^{*}p < 0.05$. (For interpretation of the references to color in this figure legend, the reader is referred to the web version of this article.)

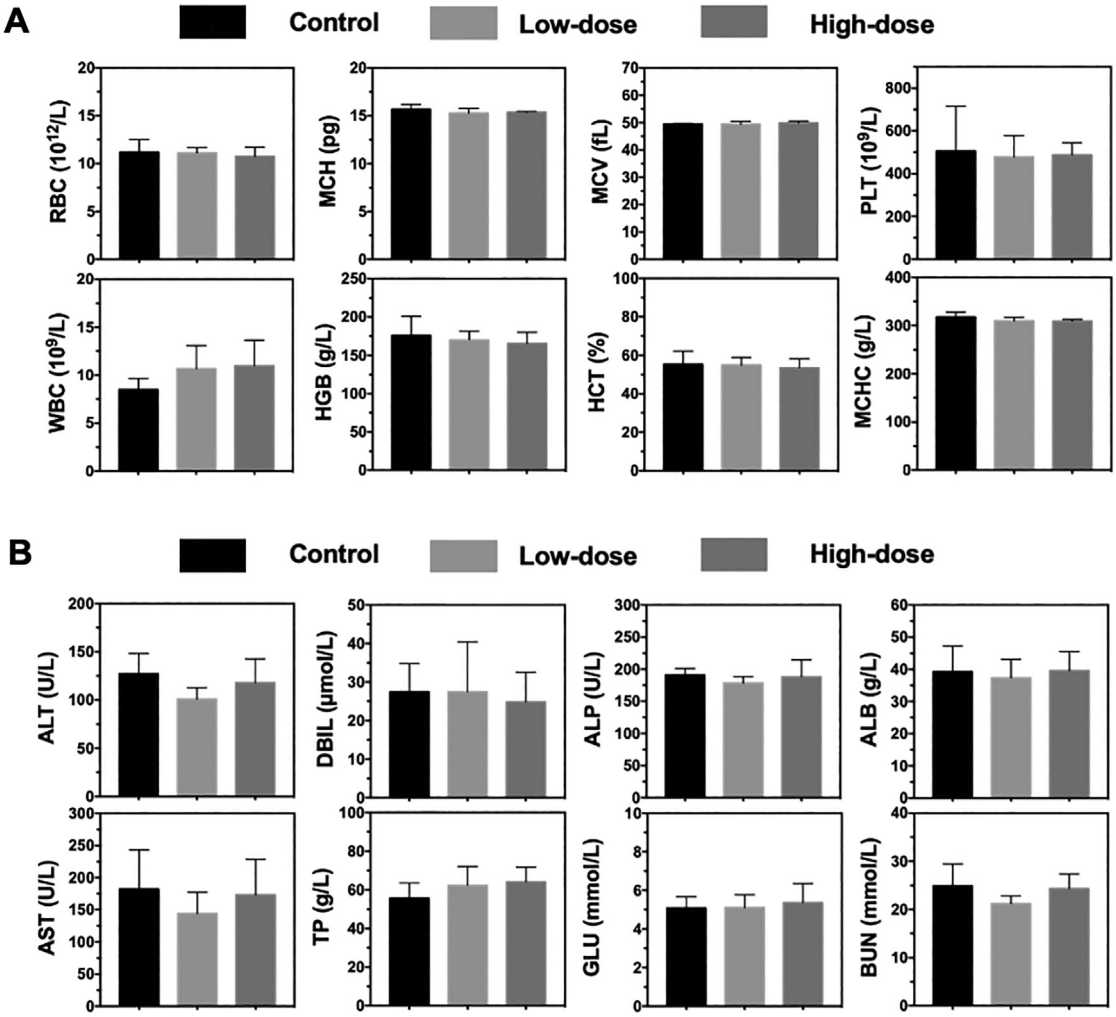

Fig. 6. (A) Hematology analysis of the mice after GO-PU injection. The data were collected after 7 days injection of GO-PU. The following parameters were measured: WBC, RBC, MCV, PLT, MCH, HGB, HCT and MCHC. (B) Blood biochemistry data of the mice with GO-PU 7 days after injection. The testing parameters including ALT, AST, TP, BUN, ALB, ALP, DBIL, and GLU.

(AST), total protein (TP), blood urea nitrogen (BUN), albumin (ALB), alkaline phosphatase (ALP), direct bilirubin (DBIL), and glucose (GLU) were examined **(**Fig. 6**B)**. Similarly, there is no significant difference in each group, indicating the high biocompatibility of GO-PU. Since ALT, AST and ALP levels are usually associated with hepatic and renal functions in mice, the results confirmed that GO-PU did not cause significant hepatorenal toxicity.

For further confirmation, the histological morphology of major organs of mouse were examined. The major organs including the heart, liver, spleen, lung, and kidney are collected and sliced for H&E staining and histological examination **(**Fig. 7**)**. The results showed that there were no obvious abnormalities at either low or high doses of GO-PU compared with the control group, indicating that GO-PU does not lead to lesions in major organs of mice, which illustrates that the excellent biocompatibility of GO-PU.

For 2D materials, especially nGO-based materials, although some researchers claimed that they were biocompatible [49,50], there were many different opinions expressing their concerns [51–53]. Some studies proposed that 2D materials like nGO and black phosphorus might enter cells through endocytosis, thus causing cell damaging [54]. The accumulation of nGO in the body might also cause toxic effects based on oxidative stress [39], and the effects on potential gene expression [55,56], thus limiting the biological application of 2D materials. In general, nGO was deemed to be safer than graphene due to its higher degree of oxidation and less free electrons [57]. Moreover, some studies have shown that the effect of graphene on cells was size- and dose-dependent, and the graphene of smaller size and higher concentration was more easily taken up by cells [39,58]. In this study, the GO-PU contents in the polymeric scaffold were only 5%, while nGO contents in GO-PU were 0.1%, and its unique dispersibility allowed it to gradually disperse in the body fluid and eliminated out as the scaffold degraded, which could minimize the toxic effects of nGO; and previous studies indicating that even tiny amounts of nGO also can endow the matrix materials to biological activity [59,60]. During this process, the polyurethane GO-PU should be partially degraded to form a PEG-nGO complex [61,62]. Studies have shown that such complexes were biosafe and even more biocompatible than nGO [63,64]. Compared with nGO and other derivatives which were easy to be endocytosed, nGO-PEG could stimulate macrophages to secrete many cytokines related to cell activation without internalization, and its interaction with cell membranes not only did not destroy the integrity of the membrane, but also promoted cell migration. These evidences suggest that GO-PU is biocompatible, and the addition of GO-PU ink modifier is able to endow the matrix materials with multifunction but any toxicity.

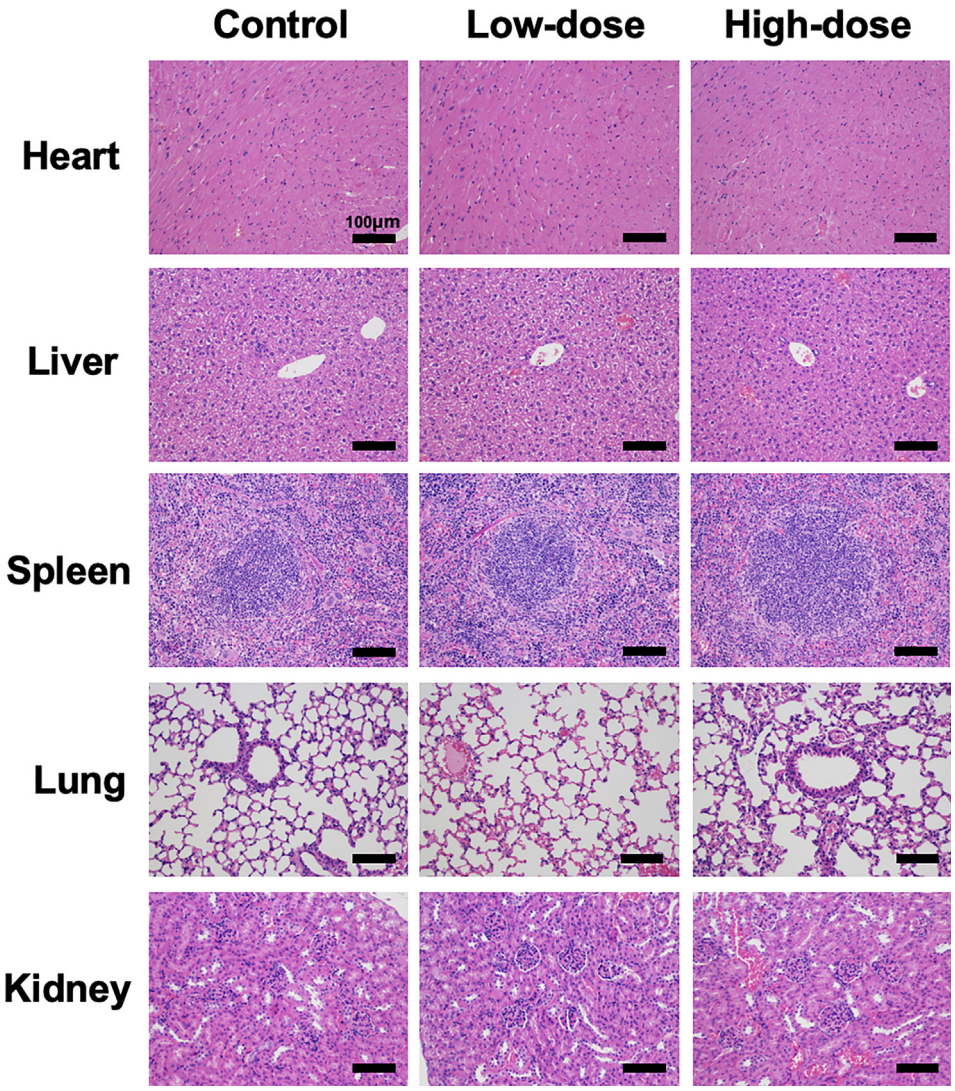

Fig. 7. Histological data acquired from the heart, liver, spleen, lung, and kidney 7 days after injection of the GO-PU.

4. Conclusion

In summary, a polyurethane GO-PU ink modifier with excellent dispersibility was successfully obtained. It was confirmed that GO-PU could be dispersed in various organic/aqueous processing solvents, enabling it to be adapted to a variety of 3D printing systems for molding and thus applied to the introduction and modification of nGO into other matrix materials. Taking PEGDA and PLGA matrix materials as examples, it was found that only 5% of GO-PU needed to be added before molding, and thus these resulting composite GO-PU based materials with better printability could be 3D-prined to fabricate a better scaffold. Further results revealed that the introduction of GO-PU could not only improve the mechanical properties and printability of the bioinks that was beneficial for 3D printing, but also endow the enhanced performances of the resulting scaffolds from the incorporated functional nGO segments, such as the mechanical properties, photo-triggered drugs release. Further, the GO-PU based materials were demonstrated with no toxicity *in vitro* and *in vivo*. Therefore, this study opens up a facile and universal approach for introduction of the emerging GO materials into 3D-printed tissue regenerative scaffolds, holding much promise in enlarging its application in tissue regeneration.

CRediT authorship contribution statement

Chengshen Hu: Conceptualization, Data curation, Formal analysis, Software, Investigation, Methodology, Writing-original draft. **Zhigang Chen:** Data curation, Investigation, Methodology. **Lan Tang:** Formal analysis, Software. **Juan Liu:** Investigation, Methodology. **Jirong Yang:** Formal analysis, Methodology, Funding acquisition. **Wing-Fu Lai:** Resources. **Tong Wu:** Methodology. **Siyuan Liao:** Software. **Xintao Zhang:** Resources, Validation, Writing-review & editing. **Haobo Pan:** Resources, Validation, Writing-review & editing. **Changshun Ruan:** Conceptualization, Funding acquisition, Supervision, Validation, Writing-original draft, Writing-review & editing.

Declaration of Competing Interest

The authors declare that they have no known competing financial interests or personal relationships that could have appeared to influence the work reported in this paper.

Acknowledgements

The authors gratefully acknowledge the support for this work from the National Key research and Development Program [Grant

No. 2018YFA0703100]; the National Natural Science Foundation of China [Grant Nos. 32122046, 82072082, 32000959, 31900959]; the Youth Innovation Promotion Association of CAS [Grant No. 2019350]; the Guangdong Natural Science Foundation (Grant Nos. 2019A1515011277, 2019A1515111197) and the Shenzhen Fundamental Research Foundation [Grant Nos. JCYJ20190812162809131, JCYJ20200109114006014, JCYJ20210324115814040 and JSGG20210629144537007].

Appendix A. Supplementary material

Supplementary data to this article can be found online at https://doi.org/10.1016/j.matdes.2022.110551.

References

[1] Y. Ma, N. Hu, J. Liu, X. Zhai, M. Wu, C. Hu, L. Li, Y. Lai, H. Pan, W.W. Lu, X. Zhang, Y. Luo, C. Ruan, Three-Dimensional Printing of Biodegradable Piperazine-Based Polyurethane-Urea Scaffolds with Enhanced Osteogenesis for Bone Regeneration, ACS Appl. Mater. Inter. 11 (9) (2019) 9415–9424, https://doi.org/10.1021/acsami.8b20323.

[2] F. Gao, Z.Y. Xu, Q.F. Liang, B. Liu, H.F. Li, Y.H. Wu, Y.Y. Zhang, Z.F. Lin, M.M. Wu, C.S. Ruan, W.G. Liu, Direct 3D Printing of High Strength Biohybrid Gradient Hydrogel Scaffolds for Efficient Repair of Osteochondral Defect, Adv. Funct. Mater. 28(13) (2018). https://doi.org/ARTN 1706644 https://doi.org/10.1002/adfm.201706644.

[3] M. Askari, M. Afzali Naniz, M. Kouhi, A. Saberi, A. Zolfagharian, M. Bodaghi, Recent progress in extrusion 3D bioprinting of hydrogel biomaterials for tissue regeneration: A comprehensive review with focus on advanced fabrication techniques, Biomaterials, Science 9 (3) (2021) 535–573, https://doi.org/10.1039/D0BM00973C.

[4] Y. Cheng, K.H. Chan, X.-Q. Wang, T. Ding, T. Li, X. Lu, G.W. Ho, Direct-Ink-Write 3D Printing of Hydrogels into Biomimetic Soft Robots, ACS Nano 13 (11) (2019) 13176–13184, https://doi.org/10.1021/acsnano.9b06144.

[5] X. Liu, H. Yuk, S. Lin, G.A. Parada, T.-C. Tang, E. Tham, C. de la Fuente-Nunez, T. K. Lu, X. Zhao, 3D printing of living responsive materials and devices, Adv. Mater. 30 (4) (2018) 1704821, https://doi.org/10.1002/adma.201704821.

[6] C.C. Chang, E.D. Boland, S.K. Williams, J.B. Hoying, Direct-write bioprinting three-dimensional biohybrid systems for future regenerative therapies, J. Biomed. Mater. Res. B Appl. Biomater. 98B (1) (2011) 160–170, https://doi.org/10.1002/jbm.b.31831.

[7] Z. Chen, D.H. Zhao, B.H. Liu, G.D. Nian, X.K. Li, J. Yin, S.X. Qu, W. Yang, 3D Printing of Multifunctional Hydrogels, Adv. Funct. Mater. 29(20) (2019). https://doi.org/ARTN 1900971 https://doi.org/10.1002/adfm.201900971.

[8] S.M. Hong, D. Sycks, H.F. Chan, S.T. Lin, G.P. Lopez, F. Guilak, K.W. Leong, X.H. Zhao, 3D Printing of Highly Stretchable and Tough Hydrogels into Complex, Cellularized Structures, Adv. Mater. 27 (27) (2015) 4035–4040, https://doi.org/10.1002/adma.201501099.

[9] X.Y. Zhai, C.Y. Hou, H.B. Pan, W.W. Lu, W.G. Liu, C.S. Ruan, Nanoclay incorporated polyethylene-glycol nanocomposite hydrogels for stimulating in vitro and in vivo osteogenesis, J. Biomed. Nanotechnol. 14 (4) (2018) 662–674, https://doi.org/10.1166/jbn.2018.2559.

[10] F. Yang, V. Tadepalli, B.J. Wiley, 3D printing of a double network hydrogel with a compression strength and elastic modulus greater than those of cartilage, ACS Biomater. Sci. Eng. 3 (5) (2017) 863–869, https://doi.org/10.1021/acsbiomaterials.7b00094.

[11] G. Siqueira, D. Kokkinis, R. Libanori, M.K. Hausmann, A.S. Gladman, A. Neels, P. Tingaut, T. Zimmermann, J.A. Lewis, A.R. Studart, Cellulose Nanocrystal Inks for 3D Printing of Textured Cellular Architectures, Adv. Funct. Mater. 27(12) (2017). https://doi.org/ARTN 1604619 https://doi.org/10.1002/adfm.201604619.

[12] S. Tarafder, S. Bose, Polycaprolactone-coated 3D printed tricalcium phosphate scaffolds for bone tissue engineering: in vitro alendronate release behavior and local delivery effect on in vivo osteogenesis, ACS Appl. Mater. Interfaces 6 (13) (2014) 9955–9965.

[13] T. Yoshida, H. Miyaji, K. Otani, K. Inoue, K. Nakane, H. Nishimura, A. Ibara, A. Shimada, K. Ogawa, E. Nishida, T. Sugaya, L. Sun, B. Fugetsu, M. Kawanami, Bone augmentation using a highly porous PLGA/beta-TCP scaffold containing fibroblast growth factor-2, J. Periodontal. Res. 50 (2) (2015) 265–273, https://doi.org/10.1111/jre.12206.

[14] B.W. Yang, J.H. Yin, Y. Chen, S.S. Pan, H.L. Yao, Y.S. Gao, J.L. Shi, 2D-Black-Phosphorus-Reinforced 3D-Printed Scaffolds:A Stepwise Countermeasure for Osteosarcoma, Adv. Mater. 30(10) (2018). https://doi.org/ARTN 1705611 https://doi.org/10.1002/adma.201705611.

[15] W.G. Wang, G. Caetano, W.S. Ambler, J.J. Blaker, M.A. Frade, P. Mandal, C. Diver, P. Bartolo, Enhancing the Hydrophilicity and Cell Attachment of 3D Printed PCL/Graphene Scaffolds for Bone Tissue Engineering, Materials 9(12) (2016). 992 https://doi.org/10.3390/ma9120992.

[16] Z.F. Lin, M.M. Wu, H.M. He, Q.F. Liang, C.S. Hu, Z.W. Zeng, D.L. Cheng, G.C. Wang, D.F. Chen, H.B. Pan, C.S. Ruan, 3D Printing of Mechanically Stable Calcium-Free Alginate-Based Scaffolds with Tunable Surface Charge to Enable Cell Adhesion and Facile Biofunctionalization, Adv. Funct. Mater. 29(9) (2019). https://doi.org/ARTN 1808439 https://doi.org/10.1002/adfm.201808439.

[17] A.H. Ambre, D.R. Katti, K.S. Katti, Biomineralized hydroxyapatite nanoclay composite scaffolds with polycaprolactone for stem cell-based bone tissue engineering, J. Biomed. Mater. Res. A 103 (6) (2015) 2077–2101, https://doi.org/10.1002/jbm.a.35342.

[18] B. Lowe, M.P. Ottensmeyer, C. Xu, Y. He, Q. Ye, M.J. Troulis, The regenerative applicability of bioactive glass and beta-tricalcium phosphate in bone tissue engineering a transformation perspective, J. Funct. Biomater. 10 (1) (2019) 16, https://doi.org/10.3390/jfb10010016.

[19] J.H. Kim, S. Lee, M. Wajahat, H. Jeong, W.S. Chang, H.J. Jeong, J.-R. Yang, J.T. Kim, S.K. Seol, Three-dimensional printing of highly conductive carbon nanotube microarchitectures with fluid ink, ACS Nano 10 (9) (2016) 8879–8887, https://doi.org/10.1021/acsnano.6b04771.

[20] W.J. Wang, Y. Zhang, L.F. Zhang, Y.H. Shi, L.M. Jia, Q. Zhang, X.H. Xu, Flexible Mn3O4 nanosheet/reduced graphene oxide nanosheet paper-like electrodes for electrochemical energy storage and three-dimensional multilayers printing, Mater. Lett. 213 (2018) 100–103, https://doi.org/10.1016/j.matlet.2017.11.025.

[21] S.Y. Yang, W.N. Lin, Y.L. Huang, H.W. Tien, J.Y. Wang, C.C.M. Ma, S.M. Li, Y.S. Wang, Synergetic effects of graphene platelets and carbon nanotubes on the mechanical and thermal properties of epoxy composites, Carbon 49 (3) (2011) 793–803, https://doi.org/10.1016/j.carbon.2010.10.014.

[22] L.J. Sweetman, S.E. Moulton, G.G. Wallace, Characterisation of porous freeze dried conducting carbon nanotube-chitosan scaffolds, J. Mater. Chem. 18 (44) (2008) 5417–5422, https://doi.org/10.1039/b809406n.

[23] S.R. Shin, Y.C. Li, H.L. Jang, P. Khoshakhlagh, M. Akbari, A. Nasajpour, Y.S. Zhang, A. Tamayol, A. Khademhosseini, Graphene-based materials for tissue engineering, Adv. Drug. Deliver. Rev. 105 (2016) 255–274, https://doi.org/10.1016/j.addr.2016.03.007.

[24] R.G. Bai, K. Muthoosamy, S. Manickam, A. Hilal-Alnaqbi, Graphene-based 3D scaffolds in tissue engineering: fabrication, applications, and future scope in liver tissue engineering, Int. J. Nanomed. 14 (2019) 5753–5783, https://doi.org/10.2147/Ijn.S192779.

[25] Z.Y. Zhang, L.H. Klausen, M.L. Chen, M.D. Dong, Electroactive Scaffolds for Neurogenesis and Myogenesis: Graphene-Based Nanomaterials, Small 14(48) (2018). https://doi.org/ARTN 1801983 https://doi.org/10.1002/smll.201801983.

[26] X.H. Jia, I. Ahmad, R. Yang, C. Wang, Versatile graphene-based photothermal nanocomposites for effectively capturing and killing bacteria, and for destroying bacterial biofilms, J. Mater. Chem. B 5 (13) (2017) 2459–2467, https://doi.org/10.1039/c6tb03084j.

[27] W. Qin, X. Li, W.W. Bian, X.J. Fan, J.Y. Qi, Density functional theory calculations and molecular dynamics simulations of the adsorption of biomolecules on graphene surfaces, Biomaterials 31 (5) (2010) 1007–1016, https://doi.org/10.1016/j.biomaterials.2009.10.013.

[28] H. Jo, M. Sim, S. Kim, S. Yang, Y. Yoo, J.H. Park, T.H. Yoon, M.G. Kim, J.Y. Lee, Electrically conductive graphene/polyacrylamide hydrogels produced by mild chemical reduction for enhanced myoblast growth and differentiation, Acta Biomater. 48 (2017) 100–109, https://doi.org/10.1016/j.actbio.2016.10.035.

[29] Y.Q. Zhang, M. Zhang, H.Y. Jiang, J.L. Shi, F.B. Li, Y.H. Xia, G.Z. Zhang, H.J. Li, Bio-inspired layered chitosan/graphene oxide nanocomposite hydrogels with high strength and pH-driven shape memory effect, Carbohyd. Polym. 177 (2017) 116–125, https://doi.org/10.1016/j.carbpol.2017.08.106.

[30] C.T. Huang, L.K. Shrestha, K. Ariga, S.H. Hsu, A graphene-polyurethane composite hydrogel as a potential bioink for 3D bioprinting and differentiation of neural stem cells, J. Mater. Chem. B 5 (44) (2017) 8854–8864, https://doi.org/10.1039/c7tb01594a.

[31] M. Kalbacova, A. Broz, J. Kong, M. Kalbac, Graphene substrates promote adherence of human osteoblasts and mesenchymal stromal cells, Carbon 48 (15) (2010) 4323–4329, https://doi.org/10.1016/j.carbon.2010.07.045.

[32] E. Nishida, H. Miyaji, H. Takita, I. Kanayama, M. Tsuji, T. Akasaka, T. Sugaya, R. Sakagami, M. Kawanami, Graphene oxide coating facilitates the bioactivity of scaffold material for tissue engineering, Jpn. J. Appl. Phys. 53(6) (2014). https://doi.org/Artn 06jd04 https://doi.org/10.7567/Jjap.53.06jd04.

[33] D. Ege, A.R. Kamali, A.R. Boccaccini, Graphene Oxide/Polymer-Based Biomaterials, Adv. Eng. Mater. 19(12) (2017). https://doi.org/ARTN 1700627 https://doi.org/10.1002/adem.201700627.

[34] S. Stankovich, D.A. Dikin, R.D. Piner, K.A. Kohlhaas, A. Kleinhammes, Y. Jia, Y. Wu, S.T. Nguyen, R.S. Ruoff, Synthesis of graphene-based nanosheets via chemical reduction of exfoliated graphite oxide, Carbon 45 (7) (2007) 1558–1565, https://doi.org/10.1016/j.carbon.2007.02.034.

[35] Y.W. Zhu, S. Murali, W.W. Cai, X.S. Li, J.W. Suk, J.R. Potts, R.S. Ruoff, Graphene and graphene oxide: synthesis, properties, and applications, Adv. Mater. 22 (35) (2010) 3906–3924, https://doi.org/10.1002/adma.201001068.

[36] S.P. Zhang, P. Xiong, X.J. Yang, X. Wang, Novel PEG functionalized graphene nanosheets: enhancement of dispersibility and thermal stability, Nanoscale 3 (5) (2011) 2169–2174, https://doi.org/10.1039/c0nr00923g.

[37] J. Zhang, W.Y. Wang, H. Peng, J.T. Qian, E.C. Ou, W.J. Xu, Water-soluble graphene dispersion functionalized by Diels-Alder cycloaddition reaction, J. Iran. Chem. Soc. 14 (1) (2017) 89–93, https://doi.org/10.1007/s13738-016-0960-5.

[38] N. Sarlak, T.J. Meyer, Fabrication of completely water soluble graphene oxides graft poly citric acid using different oxidation methods and comparison of them, J. Mol. Liq. 243 (2017) 654–663, https://doi.org/10.1016/j.molliq.2017.08.086.

[39] Y.L. Chang, S.T. Yang, J.H. Liu, E. Dong, Y.W. Wang, A.N. Cao, Y.F. Liu, H.F. Wang, In vitro toxicity evaluation of graphene oxide on A549 cells, Toxicol. Lett. 200 (3) (2011) 201–210, https://doi.org/10.1016/j.toxlet.2010.11.016.
[40] H.Y. Mi, X. Jing, B.N. Napiwocki, B.S. Hagerty, G.J. Chen, L.S. Turng, Biocompatible, degradable thermoplastic polyurethane based on polycaprolactone-block-polytetrahydrofuran-block-polycaprolactone copolymers for soft tissue engineering, J. Mater. Chem. B 5 (22) (2017) 4137–4151, https://doi.org/10.1039/c7tb00419b.
[41] Y.Z. Du, J. Ge, Y.N. Li, P.X. Ma, B. Lei, Biomimetic elastomeric, conductive and biodegradable polycitrate-based nanocomposites for guiding myogenic differentiation and skeletal muscle regeneration, Biomaterials 157 (2018) 40–50, https://doi.org/10.1016/j.biomaterials.2017.12.005.
[42] E. García-Tuñon, S. Barg, J. Franco, R. Bell, S. Eslava, E. D'Elia, R.C. Maher, F. Guitian, E. Saiz, Printing in Three Dimensions with Graphene, Adv. Mater. 27 (10) (2015) 1688–1693, https://doi.org/10.1002/adma.201405046.
[43] Q. Zhang, F. Zhang, S.P. Medarametla, H. Li, C. Zhou, D. Lin, 3D Printing of Graphene Aerogels, Small 12 (13) (2016) 1702–1708, https://doi.org/10.1002/smll.201503524.
[44] X. Tang, H. Zhou, Z. Cai, D. Cheng, P. He, P. Xie, D.i. Zhang, T. Fan, Generalized 3D Printing of Graphene-Based Mixed-Dimensional Hybrid Aerogels, ACS Nano 12 (4) (2018) 3502–3511, https://doi.org/10.1021/acsnano.8b00304.
[45] R.A. Jain, The manufacturing techniques of various drug loaded biodegradable poly(lactide-co-glycolide) (PLGA) devices, Biomaterials 21(23) (2000) 2475–2490. https://doi.org/10.1016/S0142-9612(00)00115-0.
[46] H. Zhang, L. Wang, L.i. Song, G. Niu, H. Cao, G. Wang, H. Yang, S. Zhu, Controllable Properties and Microstructure of Hydrogels Based on Crosslinked Poly(ethylene glycol) Diacrylates with Different Molecular Weights, J. Appl. Polym. Sci. 121 (1) (2011) 531–540, https://doi.org/10.1002/app.33653.
[47] K.Y. Lee, D.J. Mooney, Hydrogels for tissue engineering, Chem. Rev. 101 (7) (2001) 1869–1879, https://doi.org/10.1021/cr000108x.
[48] M. Shirzad, A. Zolfagharian, A. Matbouei, M. Bodaghi, Design, evaluation, and optimization of 3d printed truss scaffolds for bone tissue engineering, J. Mech. Behav. Biomed. Mater. 120 (2021) 104594, https://doi.org/10.1016/j.jmbbm.2021.104594.
[49] K. Yang, L.Z. Feng, X.Z. Shi, Z. Liu, Nano-graphene in biomedicine: theranostic applications, Chem. Soc. Rev. 42 (2) (2013) 530–547, https://doi.org/10.1039/c2cs35342c.
[50] S. Aznar-Cervantes, J.G. Martinez, A. Bernabeu-Esclapez, A.A. Lozano-Perez, L. Meseguer-Olmo, T.F. Otero, J.L. Cenis, Fabrication of electrospun silk fibroin scaffolds coated with graphene oxide and reduced graphene for applications in biomedicine, Bioelectrochemistry 108 (2016) 36–45, https://doi.org/10.1016/j.bioelechem.2015.12.003.
[51] P.P. Jia, T. Sun, M. Junaid, L. Yang, Y.B. Ma, Z.S. Cui, D.P. Wei, H.F. Shi, D.S. Pei, Nanotoxicity of different sizes of graphene (G) and graphene oxide (GO) in vitro and in vivo, Environ. Pollut. 247 (2019) 595–606, https://doi.org/10.1016/j.envpol.2019.01.072.
[52] Z. Clemente, V.L.S.S. Castro, L.S. Franqui, C.A. Silva, D.S.T. Martinez, Nanotoxicity of graphene oxide: Assessing the influence of oxidation debris in the presence of humic acid, Environ. Pollut. 225 (2017) 118–128, https://doi.org/10.1016/j.envpol.2017.03.033.
[53] A.B. Seabra, A.J. Paula, R. de Lima, O.L. Alves, N. Duran, Nanotoxicity of Graphene and Graphene Oxide, Chem. Res. Toxicol. 27 (2) (2014) 159–168, https://doi.org/10.1021/tx400385x.
[54] R. Vacha, F.J. Martinez-Veracoechea, D. Frenkel, Receptor-Mediated Endocytosis of Nanoparticles of Various Shapes, Nano Lett. 11 (12) (2011) 5391–5395, https://doi.org/10.1021/nl2030213.
[55] E. Hashemi, O. Akhavan, M. Shamsara, R. Rahighi, A. Esfandiar, A.R. Tayefeh, Cyto and genotoxicities of graphene oxide and reduced graphene oxide sheets on spermatozoa, RSC Adv. 4 (52) (2014) 27213–27223, https://doi.org/10.1039/c4ra01047g.
[56] O. Akhavan, E. Ghaderi, H. Emamy, F. Akhavan, Genotoxicity of graphene nanoribbons in human mesenchymal stem cells, Carbon 54 (2013) 419–431, https://doi.org/10.1016/j.carbon.2012.11.058.
[57] W.D. Zhang, L. Yan, M. Li, R.S. Zhao, X. Yang, T.J. Ji, Z.J. Gu, J.J. Yin, X.F. Gao, G.J. Nie, Deciphering the underlying mechanisms of oxidation-state dependent cytotoxicity of graphene oxide on mammalian cells, Toxicol. Lett. 237 (2) (2015) 61–71, https://doi.org/10.1016/j.toxlet.2015.05.021.
[58] Y.B. Zhang, S.F. Ali, E. Dervishi, Y. Xu, Z.R. Li, D. Casciano, A.S. Biris, Cytotoxicity Effects of Graphene and Single-Wall Carbon Nanotubes in Neural Phaeochromocytoma-Derived PC12 Cells, ACS Nano 4 (6) (2010) 3181–3186, https://doi.org/10.1021/nn1007176.
[59] S.K. Ghorai, S. Maji, B. Subramanian, T.K. Maiti, S. Chattopadhyay, Coining attributes of ultra-low concentration graphene oxide and spermine: An approach for high strength, anti-microbial and osteoconductive nanohybrid scaffold for bone tissue regeneration, Carbon 141 (2019) 370–389.
[60] C.S.D. Cabral, S.P. Miguel, D. de Melo-Diogo, R.O. Louro, I.J. Correia, Green reduced graphene oxide functionalized 3D printed scaffolds for bone tissue regeneration, Carbon 146 (2019) 513–523.
[61] G.T. Howard, Biodegradation of polyurethane: a review, Int. Biodeter. Biodegr. 49(4) (2002) 245-252. https://doi.org/Pii S0964-8305(02)00051-3.
[62] L. Tatai, T.G. Moore, R. Adhikari, F. Malherbe, R. Jayasekara, I. Griffiths, P.A. Gunatillake, Thermoplastic biodegradable polyurethanes: The effect of chain extender structure on properties and in-vitro degradation, Biomaterials 28 (36) (2007) 5407–5417, https://doi.org/10.1016/j.biomaterials.2007.08.035.
[63] N. Luo, D. Ni, H. Yue, W. Wei, G.H. Ma, Surface-Engineered Graphene Navigate Divergent Biological Outcomes toward Macrophages, ACS Appl. Mater. Inter. 7 (9) (2015) 5239–5247, https://doi.org/10.1021/am5084607.
[64] L. Wang, D.L. Yu, R. Dai, D. Fu, W.Z. Li, Z.M. Guo, C.H. Cui, J.Q. Xu, S. Shen, K. Ma, PEGylated doxorubicin cloaked nano-graphene oxide for dual-responsive photochemical therapy, Int. J. Pharmaceut. 557 (2019) 66–73, https://doi.org/10.1016/j.ijpharm.2018.12.037.